IEEE Access
Multidisciplinary | Rapid Review | Open Access Journal

IEEE POWER & ENERGY SOCIETY SECTION

Received February 4, 2022, accepted February 26, 2022, date of publication February 28, 2022, date of current version March 10, 2022.

Digital Object Identifier 10.1109/ACCESS.2022.3155668

A Model Predictive Control Strategy for Performance Improvement of Hybrid Energy Storage Systems in DC Microgrids

SEYYED ALI GHORASHI KHALIL ABADI, (Graduate Student Member, IEEE), SEYED IMAN HABIBI, (Graduate Student Member, IEEE), TOHID KHALILI, (Graduate Student Member, IEEE), AND ALI BIDRAM, (Senior Member, IEEE)

Department of Electrical and Computer Engineering, The University of New Mexico, Albuquerque, NM 87131, USA

Corresponding author: Seyyed Ali Ghorashi Khalil Abadi (ghorashi@unm.edu)

This work was supported by the National Science Foundation New Mexico Established Program to Stimulate Competitive Research (EPSCoR) Program under Award OIA-1757207.

ABSTRACT Filtration-based (FB) power/current allocation of battery-supercapacitor (SC) hybrid energy storage systems (HESSs) is the most common approach in DC microgrid (MG) applications. In this approach, a low-pass or a high-pass filter is utilized to decompose the input power/current of HESS into high-frequency and low-frequency components and then assign the high-frequency parts to SC. Moreover, to avoid the state of charge violation (SoC) of SC, this approach requires a rule-based supervisory controller which may result in the discontinuous operation of SC. This paper first provides a small-signal stability analysis to investigate the impact of an FB current allocation system on the dynamic stability of an islanded DC MG in which a grid-forming HESS supplies a constant power load (CPL). Then, it shows that the continuous operation of SC is essential if the grid-forming HESS is loaded by large CPLs. To address this issue, this paper proposes a model predictive control (MPC) strategy that works in tandem with a high-pass filter to perform the current assignment between the battery and SC. This approach automatically restores the SoC of SC after sudden load changes and limits its SoC variation in a predefined range, so that ensure the continuous operation of SC. As a result, the proposed FB-MPC method indirectly enables the MG's proportional-integral (PI) voltage controller to operate with higher gain values leading to better transient response and voltage quality. The performance of the proposed approach is then validated by simulating the system in MATLAB/Simulink.

INDEX TERMS Filtration-based power/current allocation systems, battery/supercapacitor hybrid energy storage systems, model predictive control, stability analysis, state of charge recovery.

NOMENCLATURE

A. ABREVIATIONS

BESS	Battery energy storage system.
CPL	Constant power load.
CPS	Constant power source.
DC	Direct current.
DER	Distributed energy resources.
ECR	Equal concern for relaxation error.
EMS	Energy management system.
FB	Filtration based.
HESS	Hybrid energy storage system.
HPF	High pass filter.
IAE	Integral of absolute error.
ISE	Integral of squared error.
LTI	Linear time invariant.
MG	Microgrid.
MPC	Model predictive control.
MPPT	Maximum power point tracking.
PPL	Pulsed power load.
PV	Photovoltaic.
SC	Supercapacitor.
SoC	State of charge.
SAVC	Sum of absolute voltage changes.

B. SYMBOLS

C_{bus}	Equivalent capacitance of the MG DC bus.
C_{SC}	Capacitance of the SC.

The associate editor coordinating the review of this manuscript and approving it for publication was Suman Maiti.

d_1	Duty cycle of the BESS converter.
d_2	Duty cycle of the SC converter.
d_{com}	Compensation term added/subtracted to/from the SC/BESS reference current.
e_{int1}	Integral of the error in BESS current controller.
e_{int2}	Integral of the error in SC current controller.
e_{int3}	Integral of the error in MG voltage controller.
H_c	MPC control horizon.
H_p	MPC prediction horizon.
I_n	Nominal current of the HESS.
i_{CP}	Resultant current of the CPL and CPS.
i_{com}	MPC compensation current.
i_{HESS}	HESS output current.
i_{HPF}	Output current of the high-pass filter.
i_{L1}	Inductor current of the BESS.
i_{L2}	Inductor current of the SC.
i_{Load}	Load current.
i_{PV}	PV output current.
i_{ref}	Reference current of the HESS computed by the voltage controller.
i_{ref}^{b}	Reference current of the BESS.
i_{ref}^{SC}	Reference current of the SC.
k_{P1}	Proportional gain of the BESS current controller.
k_{P2}	Proportional gain of the SC current controller.
k_{P3}	Proportional gain of the HESS voltage controller.
k_{I1}	Integral gain of the BESS current controller.
k_{I2}	Integral gain of the SC current controller.
k_{I3}	Integral gain of the HESS voltage controller.
L_1	Inductance of the BESS converter filter.
L_2	Inductance of the SC converter filter.
Q_n^b	Nominal charge of the BESS.
Q_n^{SC}	Nominal charge of the SC.
R_1	Resistance of the BESS converter filter.
R_2	Resistance of the SC converter filter.
R_b	Internal series resistant of the BESS.
R_{SC}	Internal series resistant of the SC.
$SoC_{\max}$	Maximum allowable SoC for SC.
$SoC_{\min}$	Minimum allowable SoC for SC.
SoC_{ref}	Reference SoC of the SC.
SoC_{SC}	SoC of the SC.
T_S	Sampling time of the MPC controller.
v_b	Terminal voltage of the BESS.
v_{ref}	Reference voltage of the voltage controller.
v_{SC}	Terminal voltage of SC.
ε	Slack variable in MPC cost function.
λ	ECR value.
ρ	Slack variable weight.
τ_d	Time delay.
τ_f	Time constant of the HPF.
ψ_e	Tracking's error weight.
ψ_c	Manipulated variable move weight.

I. INTRODUCTION

A. LITERATURE REVIEW

Microgrids (MGs) are independent active distribution networks that can enhance the performance of traditional power systems through increasing consumer participation, sustainable energy resources penetration, power system stability, and grid resiliency [1], [2]. Recently, DC MGs have gained significant attention because of their lower power conversion losses and less control complexity compared to the AC MGs. DC MGs can be considered as viable solutions for rural electrification, resilience enhancement of power grids, and supporting local energy communities [3]. However, control of DC MGs can be challenging in the presence of constant power loads (CPLs) and pulsed power loads (PPLs) which require a fast dynamic response and a large stability margin of the control system [4]–[6]. To tackle this challenge, highly-dispatchable distributed energy resources (DERs) as well as advanced control and management techniques are required to improve the transient response, stability, and flexibility of the system [7].

Battery energy storage systems (BESSs) are one of the most popular energy storages devices for MG applications. BESSs are dispatchable, with low energy losses, and comparatively low costs. Moreover, they have a high energy density that makes them suitable for peak shaving and steady-state power balancing [8], [9]. However, the BESSs may have relatively poor transient response during fast load changes due to their low power density [7], [10]. Consequently, grid-forming BESSs may not provide acceptable performance and voltage quality for a DC MG in the presence of PPLs. In addition, BESSs have a limited lifecycle. Therefore, the instantaneous variations of the renewable power generation or load power fluctuations may result in frequent charge/discharge of the batteries that lessens the BESSs' lifetime [10], [11].

The above-mentioned limitations of BESSs can be addressed by an effective combination of BESSs with supercapacitors (SCs) [7], [12]. In comparison to the BESSs, the SCs have a higher power density and faster dynamic response. So, they can release/absorb more energy for a significantly shorter time frame. Furthermore, they have a much higher lifecycle than BESSs. Thus, the frequent charge/discharge of SCs does not affect their lifetime. However, SCs are not appropriate for long-term energy storage applications because of their low energy density [13]. Considering the structural capabilities and limitations of BESSs and SCs, an SC is utilized in tandem with a BESS in battery-supercapacitor hybrid energy storage systems (HESSs) to improve the dynamic performance of the system and expand the lifespan of the BESSs. To this end, the BESS is used for steady-state power balancing while the SC absorbs transient power fluctuation from loads (e.g., PPLs) or renewable resources (e.g., PV or wind) [10].

The HESSs consisting of a BESS and SC can be designed with different topologies including passive, semi-active, and active topologies among which the active topologies are more desirable because of their higher controllability. In addition,

the full dispatch capacity of BESS and SC can be utilized in active topologies [11]. In these topologies, each of the HESS components (i.e., the BESS and SC) is connected to the MG DC bus through a power electronic converter and has an independent current control system. However, a more advanced control and energy management system (EMS) should be implemented to justify the additional costs of the active components (e.g., power electronic converters) [14].

The effective and reliable operation of the HESSs requires the design of suitable offline and online management and control algorithms. In offline methods, different optimization algorithms (e.g., stochastic programming or genetic algorithms) can be implemented to compute the suitable size of the SC, BESS and other DERs, based on the availability of renewable energy sources (e.g., wind or PV), cost of system's equipment, and the demanded power by the loads. On the other hand, online algorithms are necessary to ensure efficient and reliable real-time operation of the system. The real-time management and control strategies can be implemented in different control layers of the MG for different purposes. For instance, they can be implemented in the tertiary level of the MG for the optimal (or economic) state of charge (SoC) management of the BESSs or they can be employed in the secondary control layer of the MG for real-time power sharing between the HESS components (i.e., the BESS and SC) and other DERs. They can be also implemented in the primary control layer for effective current sharing between the BESS and SC to improve the transient voltage stability and voltage quality of the MG [11].

In DC MG applications, a HESS operates as a grid-following unit if the DC MG is connected to the utility grid, or it may operate as a grid-forming unit when the DC MG is islanded. In grid-connected mode of the MG, the voltage of the DC MG is regulated through connection to the upper hand AC grid using a bidirectional AC to DC converter. In this case, the HESS operates in power (or current) control mode, so its operation does not impact the transient voltage stability of the MG. In this operating mode, the EMS (i.e., the tertiary control layer) of the MG computes a reference power for the BESS and SC to charge the BESS with a steady power and absorb the instantaneous power fluctuations by SC. To this end, real-time optimization-based energy management strategies can be applied at the tertiary level of the MG to perform optimal power allocation between the HESS components as well as minimizing the operational cost of the MG. To this end, the real-time optimal EMS strategies usually considers the mid-term operation of the system (e.g., within a few hours' time interval) while the fast dynamics of the system related to primary-level controllers and power electronic converters are neglected [11], [15].

In grid-forming operation (i.e., the islanded mode of the MG), the HESS module is responsible for maintaining the dynamic stability and voltage quality of the DC MG. In this case, the HESS receives a reference current signal that is typically computed by a proportional-integral (PI) voltage controller to regulate the voltage of the MG DC bus. So, the HESS power/current allocation system may interact with the primary-level controllers including the voltage controller and current regulators of the BESS and SC converters. As a result, the HESS actions may indirectly affect the voltage quality and transient response of the system. Thus, compared to grid-following operation, the HESS power/current allocation system should have a significantly faster dynamic response to effectively share the HESS reference current computed by the MG voltage controller between the SC and BESS [7], [16], [17].

Filtration-based (FB) power/current allocation of HESSs is the most common approach in MG applications that can be implemented for both grid-following and grid-forming HESS units. FB strategies have low computational complexity making them a feasible solution for real-time applications, e.g., for grid-forming HESS units [11], [18]. In this approach, the HESS control system utilizes a low-pass, or a high pass filter to split the HESS reference current/power into high frequency and low-frequency components and then allocates the high-frequency parts into SC and the low-frequency components to BESS (i.e., "BESS-SC" operating mode). Considering the fact that SC has a low energy density and a small charge time (e.g., in the range of a few seconds), it can be immediately fully charged/discharged after a sudden load variation. However, the conventional FB strategies cannot automatically limit the SoC variation of SC (and its terminal voltage) in a predefined range. So, they typically employ a rule-based supervisory controller that may deactivate the filter and send the HESS reference current to the BESS (i.e., "BESS-only" operation) if the SoC of SC violates a predefined range [18]. Consequently, the continuous operation of SC is not guaranteed, and the HESS may frequently switch between different operating modes to limit the SC SoC variation in a predefined range. However, these switching instances may trigger some transient voltage deviations during the system operation and affect the voltage quality of MG. Moreover, this paper investigates that when a grid-forming HESS performs the "BESS-SC" mode, the MG voltage control system has higher marginal stability compared to the "BESS-only" operation. Thus, because of the destabilizing effect of CPLs, it is essential to guarantee the continuous operation of SC, particularly, if the grid-forming HESS is loaded by a large CPL.

In practice, to ensure the continuous operation of SC, the size of SC should be enough large to handle the significant power/current variations which in turn increases the initial cost of the system; or the cut-off frequency of the filter should be reduced, thereby decreasing the BESS's lifetime. To address this issue, the previous work of authors [19] was to develop an active compensation filtering technique that automatically recovers the SoC (or terminal voltage) of SC to significantly reduce the required number of switching instances. However, that approach still needs a rule-based

EMS that may deactivate the SC to guarantee its SoC variation in a predefined range. The proposed work in [20]

also suggests a virtual capacitance droop method that can automatically recover the SoC of SC to a reference value. It is also shown that this approach can slightly improve the marginal stability of MG given that the droop parameters are selected appropriately. However, this approach may cause a steady-state voltage deviation which is one of the intrinsic limitations of the droop control techniques [21]. Also, the right choice of droop coefficients can be a tedious task in DC MGs with multiple loads or DERs.

Recently, model predictive control (MPC) strategies have gained significant attention in HESS applications. The main idea of MPC is to utilize the dynamical model of the system to predict the system's outputs (i.e., prediction step) within a moving horizon (i.e., prediction horizon) and then compute a sequence of future control actions to minimize a predefined cost function (i.e., optimization step) [22], [23]. One of the interesting features of MPC controllers is their ability to directly apply the operational constraints in their real-time optimization step. Consequently, MPC strategies can automatically limit the SoC variation of the HESS components in a predefined range. However, they have considerably higher computational complexity compared to the rule-based approaches.

In DC MGs with HESS technologies, the MPC strategies can be applied in different control layers for different purposes. For instance, the references [24]–[28] propose MPC-based EMS of HESSs in which the MPC controllers are located at the tertiary level of the MG, and they are responsible for optimal (or economic) energy management and scheduling of different DERs including the HESS units. In such applications, the sampling time or action time of the MPC controller is typically in the range of a few minutes. So, the MPC prediction model (i.e., the prediction step) does not consider the fast dynamics of the system (e.g., primary controllers, power electronic converters, and circuit dynamics). Therefore, these methods focus on improving the steady state performance of the system and they don't address the voltage stability or transient response of the MG. In addition, at this layer, the MPC controllers typically have centralized architectures which need the information of all DERs to ensure the optimal operation of MG. Alternatively, The MPC controllers can be utilized in the primary controller layer of MG (e.g., direct MPC methods) to control the output voltage and currents of the power electronic converters [22]. For example, the reference [29] proposes a finite control set MPC (FCS-MPC) approach to improve the transient response and resiliency of a grid-forming HESS unit in a DC MG. In this approach, the FCS-MPC is located at the primary control layer of the MG, and it directly manipulates the converters' switches to regulate the output current of the BESS and SC to their reference values which are both computed by a FB power/current allocation system. However, the FCS-MPC strategies may intrinsically lead to intractable optimization problems due to their high computational complexity [23]. They also cause variable frequency switching that complicates the design of the converter's output filters [30], [31]. Additionally, the implementation of them for DC MG applications requires a major reconfiguration of the inner loop converter controllers which may not be always feasible. Fig. 1 compares the discussed real-time control and management strategies of HESSs concerning the standard control hierarchy of DC MGs.

B. CONTRIBUTION AND SCOPE

To address the discussed challenges and improve the performance of a grid-forming HESS unit in regulating the MG DC bus voltage (i.e., enhancing the performance of the MG primary control layer), this paper has the following contributions:

1) This paper develops a detailed state-space dynamic model of an islanded DC MG in which a grid-forming HESS supplies a CPL. It is also assumed that the HESS utilizes a conventional FB power/current allocation strategy with a rule-based supervisory controller.

2) It provides a small-signal stability analysis to compare the marginal stability of the MG in "BESS-SC" and "BESS-only" operating modes of the HESS. The stability analysis shows that the DC MG has significantly higher marginal stability in the "BESS-SC" operating mode. This means that if the HESS only performs the "BESS-SC" operating mode, the MG PI voltage controller can work with significantly larger gain values and remain stable for larger communication delays.

3) An FB-MPC approach is proposed in which an MPC control system works in tandem with a linear time-invariant (LTI) filter to perform the current assignment between the BESS and SC. In this approach, the MPC module automatically restores the SoC of SC after sudden load changes and ensures its SoC variation in a predefined range. As a result, the grid-forming HESS is able to always work in "BESS-SC" operating mode, so the continuous operation of SC is guaranteed. Consequently, the MG's PI voltage controller can operate with higher gain values which results in a better transient response and voltage quality, particularly, if the DC MG is loaded by large CPLs.

4) Compared to the existing MPC strategies in DC MG applications, the proposed MPC controller is unique in the sense that it is located at the primary control layer of the MG (i.e., interacts with voltage and current regulators of power electronic converters) but it is not responsible for regulating the output voltage or current of the power electronic converters. Instead, it is responsible for managing the SC SoC variation by computing a compensation term and adding/subtracting that value to/from the reference current of the BESS and SC power electronic converters. Due to this feature, it does not require to be as fast as the direct MPC methods (e.g., FCS-MPC). For instance, the action time of the proposed MPC controller can be in the range of a few milliseconds or more while the direct MPC methods action time should be less than a millisecond. So, the

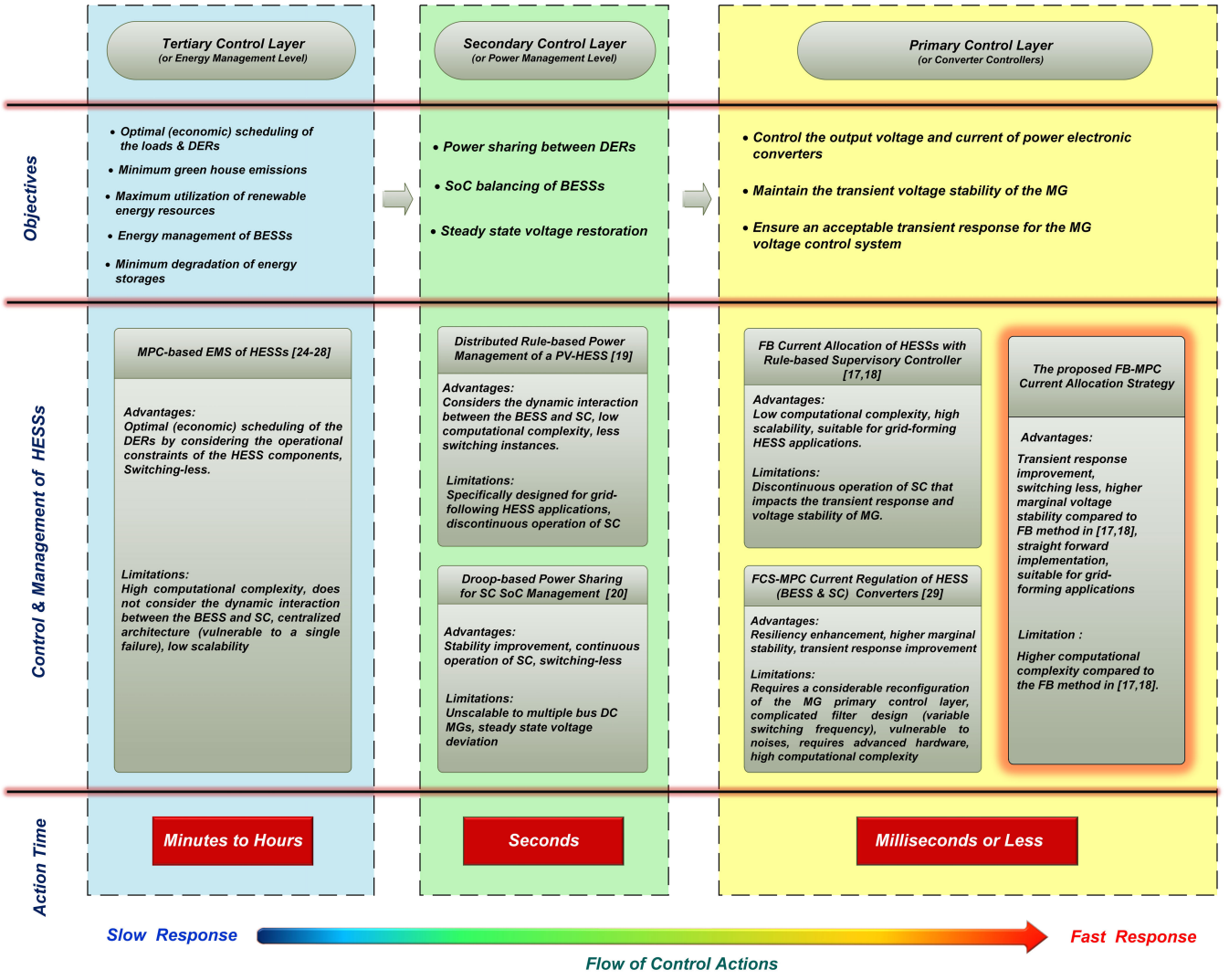

FIGURE 1. A comparison between different real-time control and management strategies of HESSs with respect to the standard hierarchical control structure of DC MGs.

optimization step is less complex in this method (i.e., more suitable for real-time applications). Moreover, its prediction model does not need the dynamics of the MG circuit model or the power electronic converters. In addition, it does not require the information of other DERs including their output currents or voltages. Instead, it just requires the filter model and the nominal current and charge capacity of the SC. Consequently, it has a considerably less complex prediction model. In addition, it can be easily adapted for the multi-generation/multi-bus DC MGs due to its decentralized architecture

It should be noted that the proposed FB-MPC approach aims to improve the performance of the MG's primary control layer. Because the primary control layer of MG has very fast dynamic responses, this work focuses on the short-term operation of the system (i.e., in the range of a few seconds) to study the transient response and voltage stability of the system under rapid load changes. So, the SoC management of BESSs that typically requires long-term (or mid-term) EMS and power sharing strategies and demands the appropriate actions of the secondary and tertiary control layer of the MG, is not discussed in this work. Fig. 1 compares the scope and contribution of this research with the discussed literature with respect to control hierarchy of DC MGs. The rest of this paper is organized as follows: Section II describes the proposed system architecture and develops the dynamical model of the DC MG to provide a small-signal stability analysis. Next, it discusses with detail how the conventional FB strategies can affect the performance of the MG voltage control system and why implementing the proposed FB-MPC method can be advantageous. Then, section III discusses the proposed MPC-based SC SoC restoration technique. The performance of the proposed FB-MPC approach is then verified through computer simulation in section IV. Section V discusses the future research directions and section VI concludes the paper.

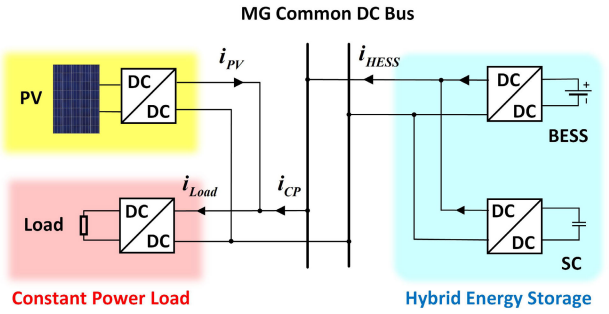

FIGURE 2. The schematic model of the case study system.

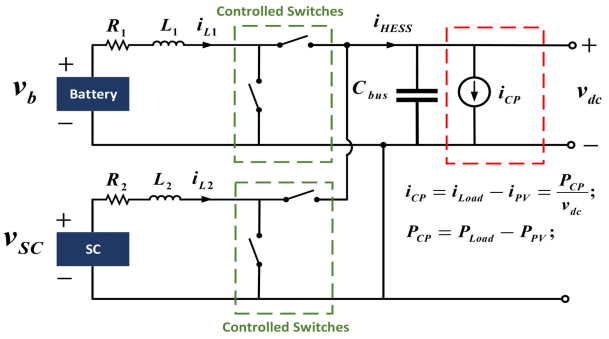

FIGURE 3. The circuit model of the case study DC MG system.

II. SYSTEM ANALYSIS

This section investigates the impact of an FB power/current allocation system on the dynamic stability of MG. Fig. 2 shows an islanded DC MG containing a PV power generation system, a HESS module, and a CPL where i_{HESS}, i_{Load}, and i_{PV} represent the HESS, load and PV currents, respectively. i_{CP} also represents the difference between the load and PV currents (i.e., $i_{CP} = i_{Load} - i_{PV}$). The case study system in this work is based on the standard single bus islanded DC MG proposed in [17], [18] in which the HESS controls the common DC bus voltage. As seen, the HESS module contains a BESS and SC which are both connected in parallel to the MG DC bus through bidirectional boost converters. The CPL is considered as a DC load connected to the MG DC bus through a power electronic converter (i.e., a load converter) and it demands a steady power under varying voltage at MG side. Here, it is assumed that the PV is in maximum power point tracking (MPPT) mode and operates as a constant power source[1] (CPS). The HESS also operates as a grid-forming unit to regulate the MG DC bus voltage.

Fig. 3 shows the equivalent circuit model of the islanded DC MG where v_b and v_{SC} are the terminal voltages of the BESS and SC. i_{L1} and i_{L2} are the output currents of the BESS and SC, and v_{dc} is the DC bus voltage. P_{CP} is also the difference between the demanded power by the CPL (i.e., P_{Load}) and the generated power by the CPS (i.e., P_{PV}). Consequently, when the PV power generation becomes larger than the demanded power by the load (i.e., $P_{CP} < 0$), the grid-forming HESS module charges by a CPS. On the other hand, if the demanded power by the load converter is higher than the PV generation power (i.e., $P_{CP} > 0$) the HESS is loaded by a CPL. It is worth noting that CPLs may degrade the dynamic stability of DC MGs due to their negative incremental resistance [32], [33]. Consequently, the DC MGs that contain large CPLs require high marginal stability of control system to ensure the reliable operation of them.

[1]In MPPT mode, the PV module generates its maximum available power regardless of the varying voltage at MG DC bus. So, it performs as a constant power source at each operating point.

TABLE 1. System parameters.

Symbol	Quantity	Value
v_{ref}	reference or nominal voltage of the DC bus	200 V
k_{P1}, k_{P2}	proportional gains of the current regulators	200
k_{I1}, k_{I2}	integral gains of the current regulators	500
L_1, L_2	inductance of the converter filter	200 µH
R_1, R_2	resistance of the converter filter	4 mΩ
C_{bus}	total capacitance of the MG DC bus	800 µF
v_b	terminal voltage of BESS	50 V
v_{SC}	terminal voltage of SC	40 V

Fig. 4 illustrates the conventional FB power allocation strategy in a grid-forming HESS unit. In this structure, the voltage regulator is a proportional-integral (PI) controller that computes a reference current (i.e., i_{ref}) for the HESS module to regulate the DC bus voltage. Next, the HESS power allocation module extracts the high frequency components of the HESS reference current (i.e., i_{ref}) using a high-pass filter (HPF). Then, to ensure the safe and reliable operation of system, the HESS current allocation system performs two modes of operation called "BESS-SC" and "BESS-only". During the "BESS-SC" operating mode (i.e., $S = 1$), the system allocates the high frequency components of the HESS reference current (i.e., i_{HPF}) to the SC (i.e., $i^{SC}_{ref} = i_{HPF}$) and the remaining low frequency components to the BESS (i.e., $i^{b}_{ref} = i_{ref} - i_{HPF}$). On the other hand, to avoid SC SoC violation, the supervisory controller may deactivate the filter (or SC) and switch to the "BESS-only" operating mode (i.e., $S = 0$). In this case, the system allocates all the reference current to the BESS (i.e., $i^{b}_{ref} = i_{ref}$, $i^{SC}_{ref} = 0$). So, the HESS operates like a single BESS when the power allocation filter is deactivated (i.e., "BESS-only" mode). The simplified logic of the rule-based supervisory controller for SC SoC management is represented in Fig. 5. Finally, at each operating mode, the current controllers calculate the duty of cycle of BESS and SC converters, i.e., d_1 and d_2, to regulate their output currents to their reference values, i.e., i^{b}_{ref} and i^{SC}_{ref}.

In what follows, section II.A develops the state space dynamical model of the closed-loop system. Then, using

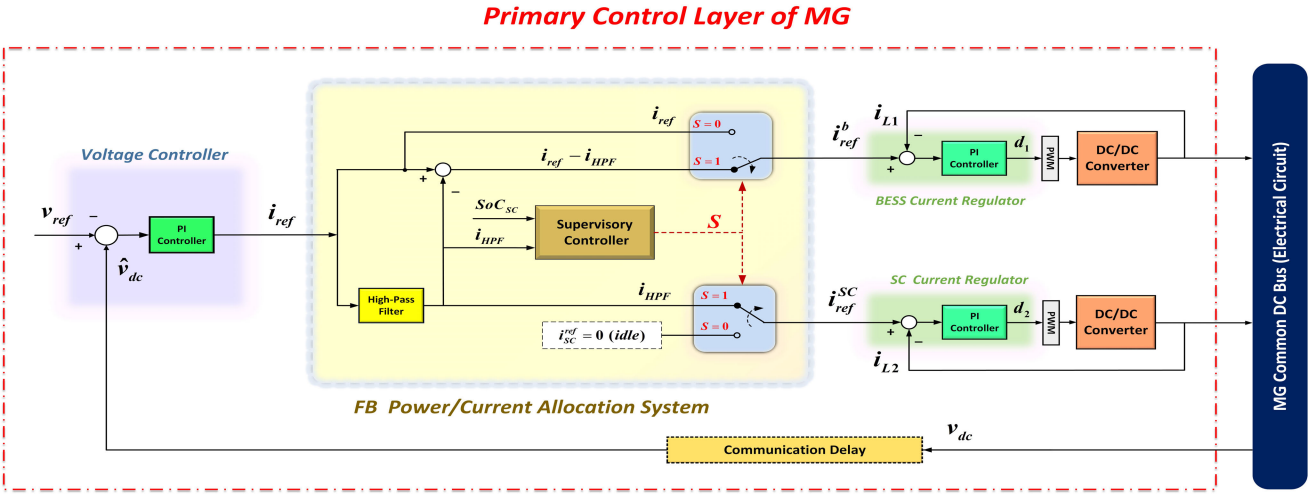

FIGURE 4. The structure of a grid-forming HESS with the conventional FB power/current allocation strategy adopted from [17], [18].

the developed dynamical model, section II.B analyzes the small-signal stability of the system to compare the marginal stability of DC MG in the two different modes of operation, i.e., "BESS-SC" and "BESS-only". It will also discuss the impact of the filter's time constant (or bandwidth) on the stability of the closed-loop system.

A. DYNAMICAL MODELING

Based on the circuit model shown in Fig. 3, and dynamic equation of single-bus DC MGs with CPLs proposed in [34] the state space averaged dynamic model of the open-loop system (i.e., the islanded single-bus DC MG) is obtained as

$$\begin{cases} L_1 \dfrac{di_{L1}}{dt} = v_b - R_1 i_{L1} - v_{dc}(1-d_1) \\ L_2 \dfrac{di_{L2}}{dt} = v_{SC} - R_2 i_{L2} - v_{dc}(1-d_2) \\ C_{bus} \dfrac{dv_{dc}}{dt} = i_{L1}(1-d_1) + i_{L2}(1-d_2) - \dfrac{P_{CP}}{v_{dc}} \end{cases} \tag{1}$$

where C_{bus} is the total capacitance of the MG DC bus. d_1 and d_2 are the duty cycle of the BESS and SC boost converters that are calculated by the PI current regulators. P_{CP} is also the difference between the generated power by the CPL and CPS (i.e., $P_{CP} = P_{Load} - P_{PV}$). Considering the proposed control structure in Fig. 4, d_1 and d_2 are derived as

$$\begin{cases} d_1 = k_{P1}(i^b_{ref} - i_{L1}) + k_{I1} e_{int1}, & e_{int1} = \int (i^b_{ref} - i_{L1})dt \\ d_2 = k_{P2}(i^{SC}_{ref} - i_{L2}) + k_{I2} e_{int2}, & e_{int2} = \int (i^{SC}_{ref} - i_{L2})dt \end{cases} \tag{2}$$

where i^b_{ref} and i^{SC}_{ref} are the reference values of the current regulators. (k_{P1}, k_{I1}) and (k_{P2}, k_{I2}) are the proportional and integral gains of the BESS's and SC's PI current controllers, respectively. e_{int1} and e_{int2} represent the integral of the errors (i.e., $i^b_{ref} - i_{L1}$ and $i^{SC}_{ref} - i_{L2}$), respectively. Assuming power/current allocation module utilizes a first order linear

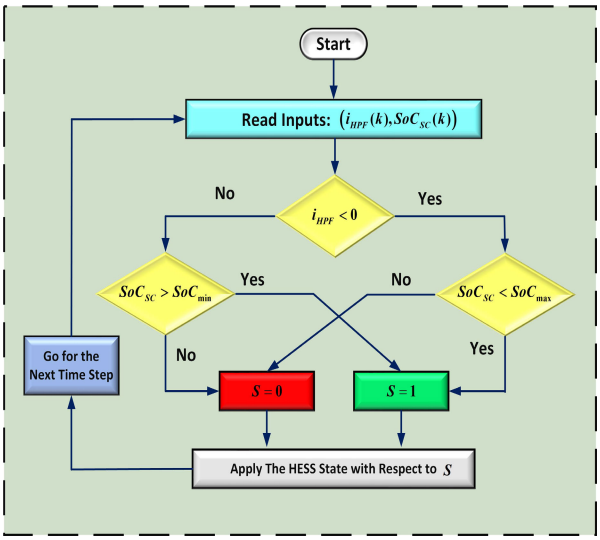

FIGURE 5. The simplified discrete logic of the HESS supervisory controller for SC SoC management. S = 1 indicates the "BESS-SC" operating mode and S = 0 indicates the "BESS-only" operation.

time invariant (LTI) filter i^b_{ref} and i^{SC}_{ref} are derived in Laplace form as

$$\begin{cases} i^b_{ref}(s) = \left(\dfrac{1}{1+\tau_f s}\right) i_{ref}(s) \\ i^{SC}_{ref}(s) = \left(\dfrac{\tau_f s}{1+\tau_f s}\right) i_{ref}(s) \\ i^{SC}_{ref} + i^b_{ref} = i_{ref} \end{cases} \tag{3}$$

where τ_f is the filter's time constant and i_{ref} is the HESS reference current. Based on (3), the performance of the current allocation system can be also explained as: If $\tau_f = (\omega_c)^{-1}$ the filter will pass the reference current (i.e., i_{ref}) from a high-pass filter with ω_c cut-off frequency to absorb the high frequency components by SC and send the remaining low-frequency components to BESS. Equation (3) can be also

represented in a state space form as

$$\begin{cases} \tau_f \dfrac{dx_f}{dt} = -x_f + i_{ref} \\ i^b_{ref} = x_f \\ i^{SC}_{ref} = i_{ref} - x_f \end{cases} \tag{4}$$

where x_f is the dynamical state of the LTI filter. The reference current, i.e., i_{ref}, is calculated by MG voltage controller and it can be represented as

$$\begin{cases} i_{ref} = k_{P3}(v_{ref} - \hat{v}_{dc}) + k_{I3} e_{int3} \\ e_{int3} = \int (v_{ref} - \hat{v}_{dc}) dt \end{cases} \tag{5}$$

where v_{ref} is the reference voltage of the MG DC bus and e_{int3} is the integral of the voltage error. k_{P3} and k_{I3} are the proportional and integral gains of the PI voltage controller. $\hat{v}_{dc}$ is also the measured DC bus voltage at the feedback loop. By assuming the feedback loop has τ_d time delay and considering a first order Padé approximation of the delay [35] (i.e., $e^{-\tau_d s} \simeq (1 - 0.5\tau_d s) / (1 + 0.5\tau_d s)$), $\hat{v}_{dc}$ is obtained as

$$\begin{cases} \dfrac{1}{2}\tau_d \dfrac{dx_d}{dt} = -x_d + v_{dc} \\ \hat{v}_{dc} = 2x_d - v_{dc} \end{cases} \tag{6}$$

where v_{dc} is the MG DC bus voltage. Thus, based on (1) to (5), the nonlinear dynamical model of the closed-loop system can be obtained as

$$\dot{x} = f(x, u) \tag{7}$$

where x represents the dynamic states of the MG (i.e., $x = [i_{L1}, i_{L2}, v_{dc}, x_d, x_f, e_{int1}, e_{int2}, e_{int3}]^T$) and $u = [v_{ref}, P_{CP}]^T$ is the input vector of the system. $f \in \mathbb{R}^8$ is a vector showing the evolution of states, and it is defined as $f = [\frac{1}{L_1} f_1, \frac{1}{L_2} f_2, \frac{1}{C_{bus}} f_3, \frac{1}{\tau_f} f_4, , \frac{2}{\tau_d} f_5, f_6, f_7, f_8]^T$ where $f_1, f_2, f_3, f_4, f_5, f_6, f_7$ and f_8 are defined in (8) to (15).

$$f_1 = v_b - R_1 i_{L1} - v_{dc} + k_{P1} v_{dc} x_f - k_{P1} v_{dc} i_{L1} + k_{I1} v_{dc} e_{int1} \tag{8}$$

$$\begin{aligned} f_2 = {} & v_{SC} - R_2 i_{L2} - v_{dc} + k_{P2} k_{P3} v_{ref} v_{dc} - 2k_{p2} k_{p3} v_{dc} x_d \\ & + k_{p2} k_{p3} v^2_{dc} + k_{P2} k_{I3} v_{dc} e_{int3} - k_{P2} v_{dc} x_f \\ & - k_{P2} v_{dc} i_{L2} + k_{I2} v_{dc} e_{int2} \end{aligned} \tag{9}$$

$$\begin{aligned} f_3 = {} & i_{L1} - k_{P1} i_{L1} x_f + k_{P1} i^2_{L1} - k_{I1} i_{L1} e_{int1} + i_{L2} \\ & - k_{P2} k_{P3} v_{ref} i_{L2} + 2k_{p2} k_{p3} x_d i_{L2} - k_{p2} k_{p3} v_{dc} i_{L2} \\ & - k_{P2} k_{I3} i_{L2} e_{int3} + k_{P2} i_{L2} x_f + k_{P2} i^2_{L2} \\ & - k_{I2} i_{L2} e_{int2} - (P_{CP}/v_{dc}) \end{aligned} \tag{10}$$

$$f_4 = -x_d + v_{dc} \tag{11}$$

$$f_5 = -x_F + k_{P3} v_{ref} - 2k_{P3} x_d + k_{P3} v_{dc} + k_{I3} e_{int3} \tag{12}$$

$$f_6 = x_f - i_{L1} \tag{13}$$

$$f_7 = k_{P3} v_{ref} - 2k_{P3} x_d + k_{P3} v_{dc} + k_{I3} e_{int3} - x_f - i_{L2} \tag{14}$$

$$f_8 = v_{ref} - 2x_d + v_{dc} \tag{15}$$

Equations (7) to (15) represent the nonlinear dynamical model of the closed-loop system in a state space form which will be used for analytically evaluating the system's stability in different modes of operation.

B. STABILITY ANALYSIS

This section analyzes the small-signal stability of the MG based on the Eigen-value analysis of the linearized system [35]. The mathematical proofs of the eigen value analysis of time-delay systems are also discussed in [36]. To this end the linearized model of the closed-loop system is obtained at each equilibrium point (i.e., Jacobian linearization). The choice of this method is justified due to high complexity of the nonlinear model. Using the nonlinear state-space equation of the system defined in (7) to (15), the stationary point of the system (i.e., $(\bar{x}, \bar{u})$) is obtained as

$$\dot{\bar{x}} = 0 \Leftrightarrow f(\bar{x}, \bar{u}) = 0 \tag{16}$$

Then, by using a first order Taylor series expansion of f and defining $\Delta x = x - \bar{x}$ and $\Delta u = u - \bar{u}$, one can obtain:

$$\Delta \dot{x} = \dot{x} - \dot{\bar{x}} = f(x, u) \simeq A_{|(\bar{x},\bar{u})} \Delta x + B_{|(\bar{x},\bar{u})} \Delta u \tag{17}$$

where A and B are defined in (18) and (19), respectively.

$$A_{|(\bar{x},\bar{u})} = \left. \frac{\delta f(x, u)}{\delta x} \right|_{(\bar{x},\bar{u})} \tag{18}$$

$$B_{|(\bar{x},\bar{u})} = \left. \frac{\delta f(x, u)}{\delta u} \right|_{(\bar{x},\bar{u})} \tag{19}$$

Consequently, to find the closed-loop poles of the linearized system at each operating point, it is required to calculate the eigenvalues of the Jacobian matrix, i.e., A, which is obtained as:

$$Eig(A) = \{\lambda \,|\det(\lambda I - A) = 0\} \tag{20}$$

In this section, firstly the marginal stability of the DC MG in "BESS-SC" and "BESS-only" operating modes is evaluated, then the reason that the system has more stability margin in "BESS-SC" operation will be discussed. To this end, two different test cases are evaluated. The parameters of the case study system are shown in Table 1. In the first test case, it is assumed that the grid-forming HESS supplies 50kW constant power load (i.e., $P_{CP} = 50$kw). Then, the closed-loop poles of the system are obtained with respect to different values of proportional and integral gains of the MG PI voltage controller (i.e., k_{P3}, and k_{I3}). As seen in Fig. 6, the closed-loop poles of the MG are very sensitive k_{P3} value when the DC MG is in "BESS-only" operating mode. In addition, the DC MG will be destabilized if $k_{P3} > 0.49$.On the other hand, the MG remains stable for significantly larger values of k_{P3} in "BESS-SC" operation (see Fig. 6(b)).

Fig. 7 also represents the closed-loop poles of the system with respect to k_{I3} changes. As seen, the dominant poles of the closed-loop system are not very sensitive to k_{I3} values in both of the operational modes. However, the DC MG will be unstable for relatively large value of integral gain (i.e., $k_{I3} > 44.3$) in "BESS-only" operation while the system remains stable in "BESS-SC" for notably larger gains (i.e., $k_{I3} \simeq 120$) (see Fig. 7(b)).

Fig. 8 represents the closed-loop poles of the system with respect to communication delay (i.e., τ_d). As seen,

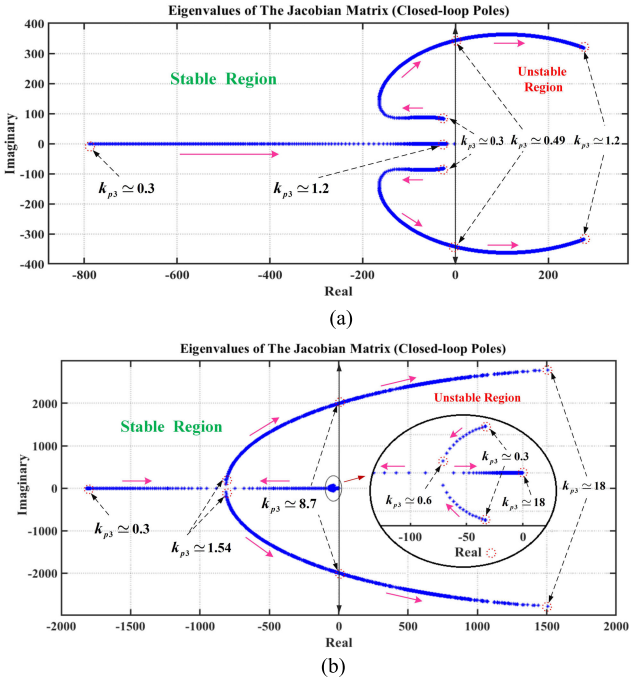

FIGURE 6. Dominant poles of the closed-loop system with respect to the proportional gain of the MG voltage controller (i.e., k_{P3}). Also, $k_{I3} = 20$, $\tau_f = 2$s, $\tau_d = 1$ms, and $P_{CP} = 50$kW. (a) "BESS-only" operation; (b) "BESS-SC" operation.

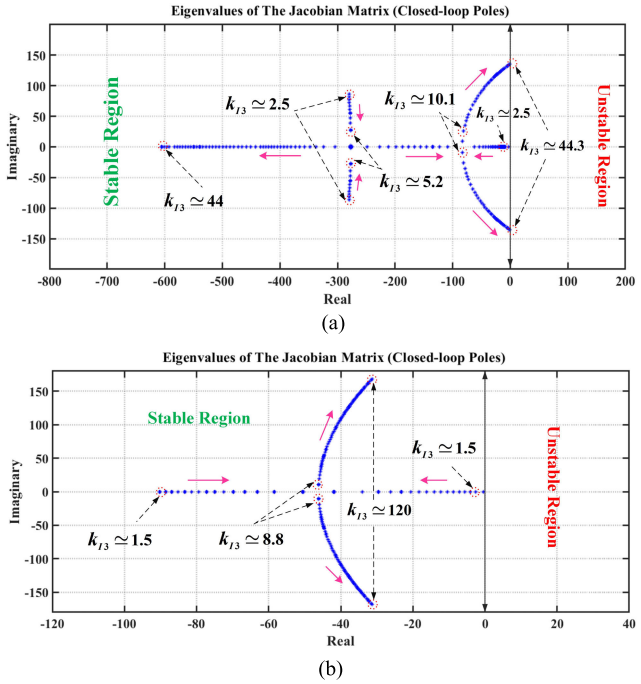

FIGURE 7. Dominant poles of the closed-loop system with respect to the integral gain of the MG voltage controller (i.e., k_{I3}). Also, $k_{P3} = 0.38$, $\tau_f = 2$s, $\tau_d = 1$ms, and $P_{CP} = 50$kW. (a) "BESS-only" operation (b) "BESS-SC" operation.

by increasing the communication delay the dominant poles of the closed-loop system move to the unstable region in both "BESS-only" and "BESS-SC" operation of the HESS.

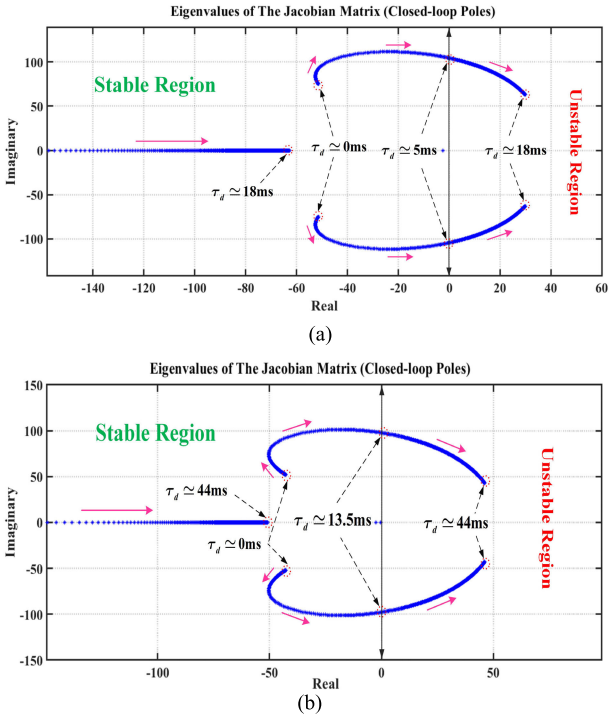

FIGURE 8. Dominant poles of the closed-loop system with respect to the communication delay (i.e., τ_d). Also, $k_{P3} = 0.38$, $k_{I3} = 20$, $\tau_f = 2$s, and $P_{CP} = 50$kW. (a) "BESS-only" operation (b) "BESS-SC" operation.

As seen in Fig.8(a), the DC MG will be unstable for the delays larger than 5 milliseconds (i.e., $\tau_d \geq 5$ms) in "BESS-only" operation and it will be destabilized for delays larger than 13.5 milliseconds (i.e., $\tau_d \geq 13.5$ms) in "BESS-SC" operation. Consequently, compared to "BESS-only" operation, the DC MG can tolerate considerably larger communication delays in "BESS-SC" operation due to its higher marginal stability at this mode.

The reason that the MG voltage controller has higher marginal stability in "BESS-SC" operating mode is directly related to the impact of current decomposition filter (i.e., the HPF) and SC operation. As seen in Fig. 4, when the HESS performs the "BESS-SC" operation, the SC is responsible for absorbing the transient power/current fluctuations to regulate the MG DC bus voltage while the BESS absorbs/releases the steady state power. To this end, the reference current calculated by the voltage controller firstly passes from the HPF, then it is sent to the SC current regulator. The HPF causes a positive phase shift (e.g., like a lead compensator) that pushes the closed-loop poles of the system to the left-side of the $j\omega$ axis (i.e., the stable region). As a result, the current decomposition filter (i.e., the HPF) improves the marginal stability of the system by acting like an active compensator. Fig. 9 illustrates the impact of the HPF time constant (i.e., τ_f) on the dynamic stability of the MG given that the HESS is loaded by a large CPL (i.e., $P_{CP} = 50$kw). In this case, based on equation (3), when the filter time's constant is very small (i.e., $\tau_f \simeq 0$), the current allocation filter (i.e., the HPF) is approximately deactivated, hence all the HESS reference

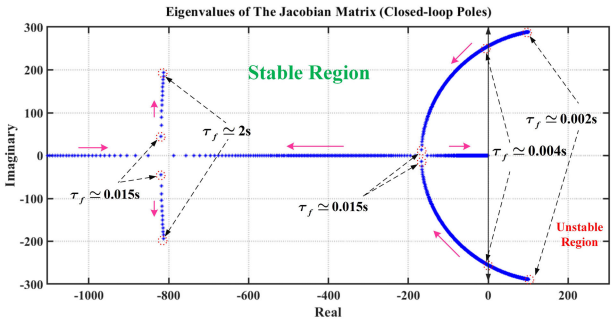

FIGURE 9. Dominant poles of the closed-loop system in "BESS-SC" operation with respects to filter's time constant (i.e., τ_f). Also $k_{p3} = 1.8$, $k_{I3} = 20$, $\tau_d = 1$ms, and $P_{CP} = 50$kW.

current is absorbed by the BESS and the SC reference current is approximately zero ($i^b_{ref} \simeq i_{ref}, i^{SC}_{ref} \simeq 0$). So, the HESS operation is similar to the "BESS-only" operating mode. On the other hand, when the filter's time constant increases, the HPF provides a wider positive phase shift, and the SC absorbs a larger portion of the HESS reference current. As seen in Fig. 9., the closed-poles of the system are pushed to the stable region and the marginal stability of system is improved by increasing the time constant of the HPF.

Regarding the provided results by small-signal stability analysis of the system one can conclude:

1) The current decomposition filter (i.e., the HPF) acts like an active compensator that improves the marginal stability of system when the HESS performs the "BESS-SC" operation. In another word, the HPF not only performs the current assignment between the BESS and SC but also improves the marginal stability of the system.
2) The system has considerably higher stability margin when SC is active (i.e., in "BESS-SC" operating mode) compared to the "BESS-only" operation. However, to ensure the voltage stability during the entire system operation, the gains of MG voltage controller should be small; otherwise, the MG may experience an unstable DC bus voltage after switching to "BESS-only" operation. On the other hand, the very low gains of the MG voltage controller may adversely affect the transient response of the system and reduce the voltage quality. Thus, the discontinuous operation of SC limits the marginal stability of the voltage controller and indirectly declines the transient response of the system.

Based on the provided results, this paper proposes an MPC strategy that works in tandem with an FB current allocation system (i.e., an HPF) to improve the performance of a grid-forming HESS. In this method, the HPF performs the current assignment between the BESS and SC as well as improving the marginal stability of the system and the MPC controller recovers the SoC of SC after sudden load changes and guarantees the continuous operation of SC. As a result, the HESS will always operate in "BESS-SC" operating mode, so the MG voltage controller can operate with higher gain values that results in a better transient response and voltage quality. Fig. 10 illustrates the justification of the proposed FB-MPC approach.

III. THE PROPOSED FB-MPC METHOD

Fig. 11 shows the proposed FB-MPC technique. In this method, similar to the FB approach, the voltage controller located at the primary control layer of the MG computes a reference current to regulate the MG common DC bus voltage. This reference current is then sent to the FB-MPC power/current allocation system. In the proposed method, the rule-based supervisory controller used in the conventional FB approach (see Fig. 3) is replaced by an MPC module (see Fig. 11), so that guarantee the continuous operation of the SC and filter. In this approach, the MPC module regulates the SoC of SC to a reference value while considering the SoC constraints of the SC. To this end, at each time step, the MPC controller employs the discretized dynamical model of the system to predict the future error between the SoC of SC and its reference value within a moving horizon, i.e., prediction horizon. Then, to minimize the error, it computes a sequence of compensation currents (i.e., i_{com}) within a moving horizon (i.e., control horizon) and applies the first one. As a result, based on the SoC variation of SC and the HESS reference current (i.e., i_{ref}), the MPC compensator sends a compensation term to the HPF. After passing from the HPF, the compensation term is added to the reference current of the SC and subtracted from the reference current of the BESS. As a result, the MPC compensator provides an additional coordination between the BESS and SC in which the BESS gradually charges/discharges the SC. Consequently, the proposed FB-MPC can control the SoC variation in a predefined range which in turn ensures the continuous operation of the SC and filter. In what follows, section III.A develops the prediction model of the MPC controller, section III.B introduces the MPC objective function, section III.C discusses the MPC tunning parameters, III.D discusses the functionality of the MPC compensator, and III.E discusses the dynamic stability of the MG under the proposed FB-MPC approach.

A. PREDICTION MODEL

The prediction model represents the dynamical relationship between the HESS refence current (i.e., i_{ref}) and the SoC of SC. The percentage value of SC's SoC can be represented as

$$SoC_{SC}(t) = \frac{-100 I_n}{Q^{SC}_n} \int_{t_0} i_{SC(p.u)} dt + SoC_{SC}(t_0) \qquad (21)$$

where Q^{SC}_n is the nominal capacity of the SC. Also, I_n and $i_{SC(p.u)}$ are the nominal and per unit value of SC's discharge current, respectively. This per unit representation is applied here for better scaling the model parameters. Assuming there is no leakage current and considering the circuit model of the system shown in Fig. 3, the discharge current is equal to the inductor current of the boost converter, i.e., $i_{SC} = i_{L2}$. In addition, knowing the fact the power electronic converter

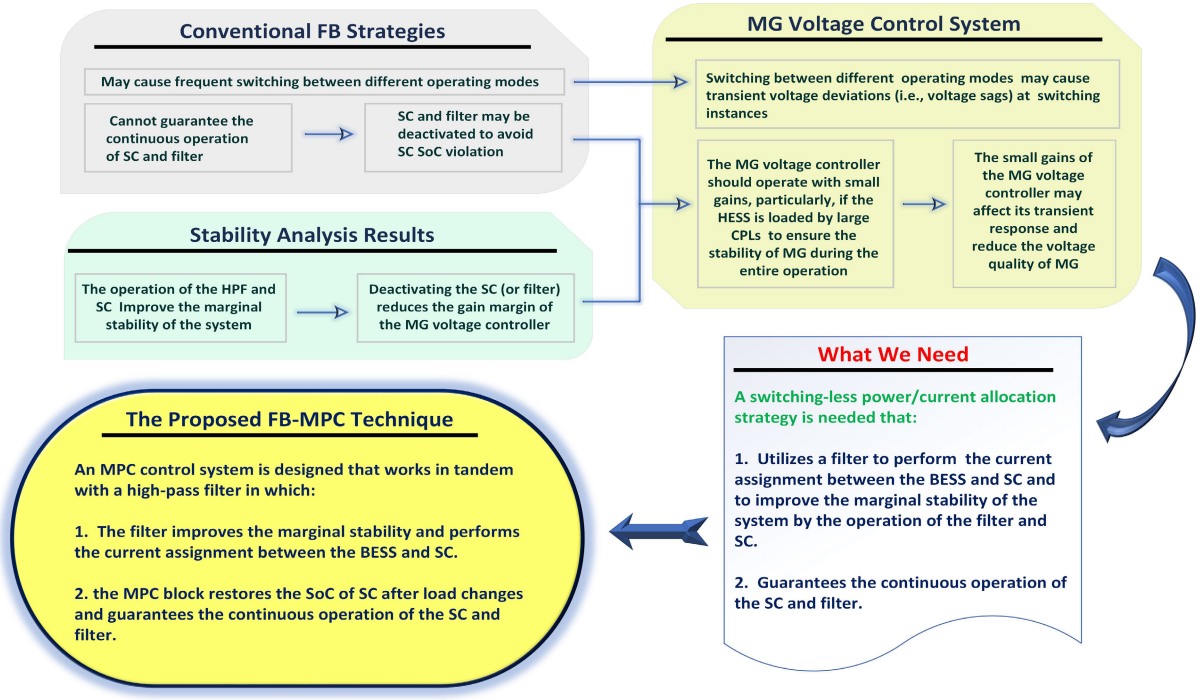

FIGURE 10. Justification of the proposed FB-MPC approach.

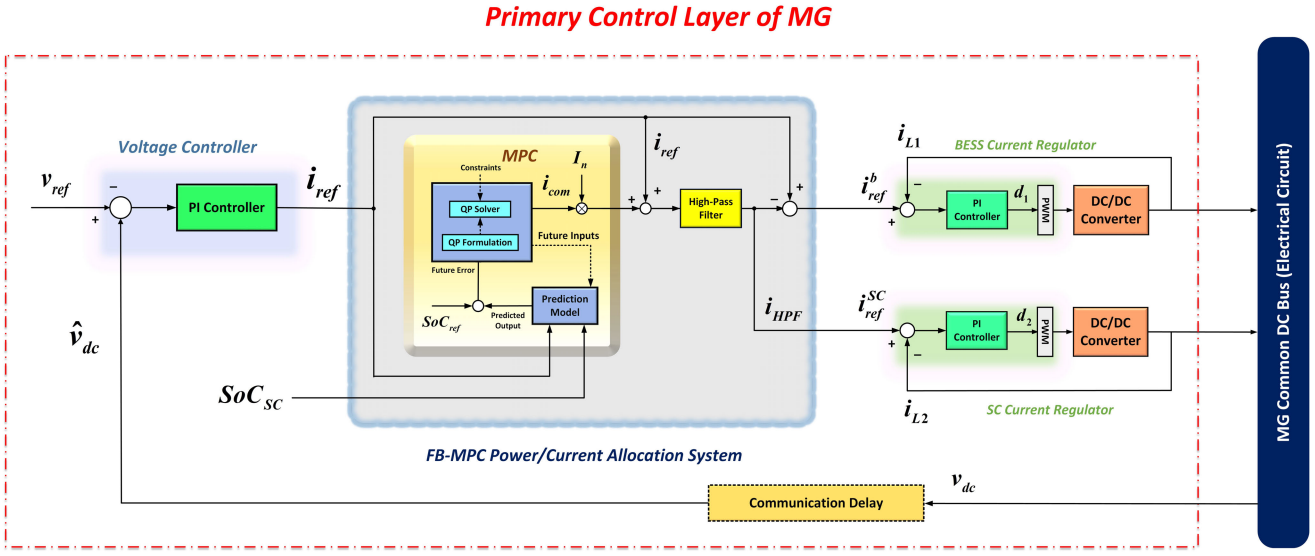

FIGURE 11. The structure of a grid-forming HESS unit with the proposed FB-MPC power/current allocation system.

and the current regulator has by far faster dynamics than SoC_{SC}, i_{L2} can be considered equal to its reference value, i.e., $i_{L2} \simeq i^{SC}_{ref}$. So, (21) can be reformulated as

$$SoC_{SC}(t) = \frac{-100I_n}{Q^{SC}_n} \int_{t_0} i^{SC}_{ref(p.u.)} dt + SoC_{SC}(t_0) \qquad (22)$$

where $i^{SC}_{ref(p.u)}$ is the per unit value of the SC's reference current. Assuming the HESS uses a first order LTI filter, $i^{SC}_{ref(p.u)}$ can be represented in Laplace form as

$$i^{SC}_{ref(p.u)}(s) = \left(\frac{1}{I_n}\right) \frac{\tau_f s}{\tau_f s + 1} i_{ref} + \frac{\tau_f s}{\tau_f s + 1} i_{com} \qquad (23)$$

where τ_f is the filter's time constant and i_{com} is the compensation current applied by the MPC compensator (see Fig. 11). Equation (23) an be also represented in a state space

form as

$$\begin{cases} \tau_f \dfrac{dx'_f}{dt} = -x'_f + i_{com} + \left(\dfrac{1}{I_n}\right) i_{ref} \\ i^{SC}_{ref(p.u)} = \left(\dfrac{1}{I_n}\right) i_{ref} + i_{com} - x'_f \end{cases} \tag{24}$$

where x'_f represents state variable of the filter's model. Using (22) and (24), the dynamical model of SC's SoC is obtained as

$$\begin{cases} \dfrac{dSoC_{SC}}{dt} = \dfrac{100 I_n}{Q^{SC}_n}\left(x'_f - i_{com}\right) - \frac{100}{Q^{SC}_n} i_{ref} \\ \dfrac{dx'_f}{dt} = \dfrac{-1}{\tau_f}\left(x'_f - i_{com}\right) + \dfrac{1}{\tau_f I_n} i_{ref} \end{cases} \tag{25}$$

The MPC compensator is naturally a discrete-time controller. So, it utilizes the discretized dynamical model of the SC's SoC. Based on (25), the MPC prediction model is represented as

$$\begin{cases} x_m(k+1) = (I + T_s A)\, x_m(k) + T_s B_1 u(k) + T_s B_2 d(k) \\ y_m(k) = C x_m(k) \end{cases} \tag{26}$$

where $x_m(k) = [SoC_{SC}(k), x'_f(k)]^T$ are the states of the prediction model, $u(k) = i_{com}(k)$ is the manipulated variable (i.e., control input), $d(k) = i_{ref}/I_n$ is the measured disturbance, I is a 2 by 2 identity matrix, and T_s is the sampling period of the MPC. Matrices A, B_1, and B_2, and vector C are

$$A = \begin{bmatrix} 0 & 100 I_n/Q^{SC}_n \\ 0 & -1/\tau_f \end{bmatrix}, \quad B_1 = B_2 = \begin{bmatrix} -100 I_n/Q^{SC}_n \\ 1/\tau_f \end{bmatrix}, \quad C = [1, 0] \tag{27}$$

B. OBJECTIVE FUNCTION

In optimization step, the MPC compensator solves a quadratic programming (QP) problem to compute the manipulated variable (i.e., compensation current) using an active set optimization method. In this QP formulation, the cost function is quadratic while the constraints have to be linear. The MPC objective function is defined as

$$\begin{aligned} \min : & \sum_{i=1}^{H_p} \psi_e \left(SoC_{ref}(k+i|k) - y_m(k+i|k)\right)^2 \\ & + \sum_{i=1}^{H_c} \psi_c \left(u(k+i|k) - u(k+i-1|k)\right)^2 + \rho \varepsilon(k)^2 \end{aligned} \tag{28}$$

$$\text{subject to the constraints:} \begin{cases} SoC_{\min} - \lambda\varepsilon(k) \le y_m(k+i|k) \\ \qquad \le SoC_{\max} + \lambda\varepsilon(k), \\ i \in \{1 \ldots, H_P\} \end{cases} \tag{29}$$

where u is the manipulated variable, y_m is the model's output represented in (28), and ε is the slack variable for constraint softening. ψ_e and ψ_c are the tunning weights on the tracking error and manipulated variable move, and ρ is constraint violation penalty weight. H_p and H_c are the prediction and control horizons and λ is equal concern for relaxation (ECR) value. It is assumed that $\lambda > 0$, $H_p > H_c$ and $u(k+i|k) - u(k+i-1|k) = 0$ for $i \ge H_c$.

C. TUNNING THE MPC PARAMETERS

The desirable operation of the MPC compensator requires appropriately tunning the MPC parameters. In (28), the first term penalizes the deviation of the SC's SoC (i.e., SoC_{SC}) from its reference value (i.e., SoC_{ref}) and the second term penalizes the rapid changes on the control input (i.e., i_{com}). The third term also penalizes a tolerable soft constraint violation compared to the other cost function terms. The tracking error has the minimum priority compared to the other terms. So, ψ_e should be considered much smaller than the ψ_c and ρ. Although a relatively large value of ρ increases the likelihood of having a very small optimal slack variable ($\varepsilon(k)$), it may result in significantly rapid manipulated variable move if the SoC constraints are violated. This rapid manipulate variable move can cause a relatively large voltage sag on the MG DC bus. Also, it may put a high stress on the BESS for charging the SC when a violation of constraints is predicted. So, the weights on the manipulated variable move should be much larger than the other cost function terms (i.e., $\psi_e \ll \rho \ll \psi_c$). Consequently, in contrast to the rule-based SC SoC compensation methods, the proposed approach can guarantee the continuous operation of SC without affecting the transient voltage of the MG (i.e., no voltage sags) by effectively tunning the MPC parameters.

D. FUNCTIONALITY OF THE MPC COMPENSATOR

As seen in Fig. 11, the MPC compensator receives the HESS reference current (i.e., i_{ref}) that is computed by the voltage controller as well as the SoC of SC (i.e., SoC_{SC}) to control the SC SoC variation in a predefined range. To this end, at the prediction step, the MPC controller employs the dynamic model of the FB current allocation system and the dynamic relationship between the SC's current and its SoC value. In this respect, the MPC controller applies the dynamic model of FB current allocation system to estimate how much of the HESS reference current will be allocated to the SC and then predicts the SC SoC variation during its prediction interval (i.e., the prediction horizon). Then, at the optimization step, the MPC controller computes a sequence of compensation terms, i.e., i_{com} (see (25) to (29)), in order to minimize the error between the SoC of SC (i.e., SoC_{SC}) and its reference value (i.e., SoC_{ref}) by considering the SC SoC constraints defined in (29). Then, the MPC controller applies the first value in the sequence and goes for the next time step. The flowchart of the MPC compensator is shown in Fig. 12.

The compensation term is then sent to the HPF. Accordingly, by assuming the DC MG including the HPF and MG voltage controller have similar dynamics to the examined case study system in section II, the reference currents of the BESS, and SC represented in (3), are reformulated in the

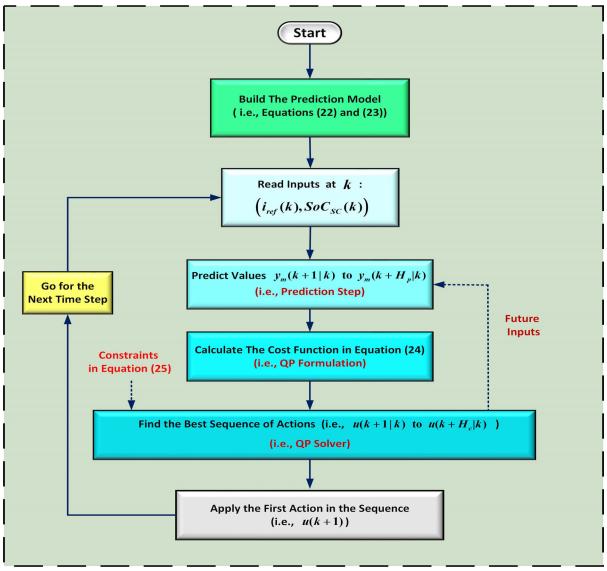

FIGURE 12. The flowchart of the proposed MPC strategy for SC SoC recovery.

FB-MPC method as

$$\begin{cases} i^{b}_{ref}(s) = \left(\dfrac{1}{1+\tau_f s}\right) i_{ref}(s) - d_{com} \\ i^{SC}_{ref}(s) = \left(\dfrac{\tau_f s}{1+\tau_f s}\right) i_{ref}(s) + d_{com} \\ i^{SC}_{ref}(s) + i^{b}_{ref}(s) = i_{ref} \end{cases} \tag{30}$$

where i_{ref} is defined in (5). d_{com} is also obtained as

$$d_{com} = (I_n)\left(\frac{\tau_f s}{1+\tau_f s}\right) i_{com} \tag{31}$$

where i_{com} is the compensation term computed by the MPC controller. As a result, the MPC controller adds a compensation term to the reference current of the SC and subtract that value from the BESS reference current. (Note: sum of the BESS and SC currents should be always equal to HESS reference current. Please also compare (3) and (30)). Consequently, the proposed FB-MPC method provides an additional coordination between the BESS and SC in which the BESS can gradually charge/discharge the SC based on the compensation term (i.e., d_{com}) that is adjusted by the MPC compensator.

It should be also noted that, fundamentally, the MPC controllers have an interesting feature which is their ability in applying the input and output constraints in their optimization step (see [22] and [23]). So, they can certify that the output or input constraints will not be violated. However, this interesting feature is not available in classical linear or nonlinear controllers. So, they cannot be as functional as the MPC methods for this application. For instance, in the proposed FB-MPC method, if the MPC compensator predicts a violation of constraints (i.e., SC SoC violation) during its prediction horizon (e.g., the MPC computes a nonzero slack variable), it can quickly adjust the d_{com} to prevent the SC SoC violation in a switching-less manner. Thus, the MPC compensator can guarantee the continuous operation of the SC and filter. In addition, the MPC compensator can limit the fast movement of the manipulated variable (i.e., i_{com}), so that reduce the stress on the BESS for charging the SC if a violation of constraints is predicted (see (28)). Consequently, from the voltage controller point view, the compensation term (i.e., d_{com}) has very slow and smooth variations which does not affect the transient voltage quality of the system.

E. VOLTAGE STABILITY OF MG WITH THE FB-MPC METHOD

As discussed in section II, the conventional FB power/current allocation strategy cannot guarantee the continuous operation of the SC and filter. Hence, the HESS may switch between two modes of operation, i.e., ''BESS-only'' and ''BESS-SC''. Then, the proposed small-signal stability analysis in II.B shows that the MG voltage control system has significantly higher marginal stability in ''BESS-SC'' operating mode compared to the ''BESS-only'' operation. Consequently, to guarantee the continuous operation of the SC and filter, an MPC controller is utilized that limits the SoC variation of SC in a predefined range. As a result, the HESS will always operate in ''BESS-SC'' operating mode. To this end, the MPC controller computes a compensation term (i.e., i_{com}) and sends it to the HPF (see Fig. 11). Accordingly, the MPC controller provides an additional coordination between the BESS and SC by adding the d_{com} to the reference current of the SC and subtract that value form the reference current of the SC (please see equation (30) and (31)).

Practically, due to the fact that the SC SoC variation has significantly slower dynamics compared to DC bus voltage, the MPC action time (or MPC sampling time) is significantly larger than the MG voltage controller (e.g., the MPC sampling time can be twenty to fifty times larger than the sampling time of the voltage controller). In addition, the variation of the MPC compensation current (i.e., the manipulated variable move) is limited in the MPC cost function (see equation (28)). As a result, from the point of view of MG voltage controller, the compensation term (i.e., d_{com}) is seen as a small disturbance that has extremely slow variations. Consequently, d_{com} does not directly change the dynamic model (e.g., the close-loop poles of the linearized model) of the MG voltage control system. Hence, in terms of dynamic stability, under the proposed FB-MPC technique, the system behaves similar to the discussed case study system in II (i.e., a grid forming HESS with conventional FB current allocation), but it always works in ''BESS-SC'' operating mode. In another word, the MPC compensator just ensures the continuous operation of SC (i.e., ''BESS-SC'' operation) in which the system has a higher marginal stability, and it does not directly affect the dynamics of the MG voltage control system.

It is also worth mentioning that the MPC control system regulates the SoC variation of the SC that impacts the terminal voltage of the SC (i.e., v_{SC}). Hence, the MPC controller may

slightly change the stationary operating point of the system (see (16) to (19)) for a specific load condition. However, v_{SC} does not appear in the small-signal model of the system, so the Jacobian Matrix and Eigen-values at similar stationary points remains unchanged. Consequently, because the range of stationary points (e.g., the allowable range for SoC of SC and v_{SC} variation) is equal in the FB-MPC and FB methods, the proposed stability analysis related to the "BESS-SC" operation of the HESS in FB approach (see section II.B), will be also valid for the FB-MPC method. Therefore, in the FB-MPC method, the voltage control system has the same stability margin compared to the "BESS-SC" operation in FB approach.

IV. SIMULATION RESULTS

This section evaluates the performance of the proposed FB-MPC technique and compares it with the conventional FB current allocation strategy by simulating these systems in MATLAB/Simulink. To this end, two test systems are compared with each other in three different load change scenarios. The test case systems have the following characteristics:

- The first system (i.e., Case 1) utilizes a conventional FB strategy represented in Fig. 4.
- The second system (i.e., Case 2) employs the proposed FB-MPC technique. The control structure of this system is illustrated in Fig. 11. The parameters of the MPC compensator are also shown in Table 2.
- The circuit parameters and the gain of PI current regulators are similar to the test cases in section II (see Table 1). Also, they use a similar LTI filter with $\tau_f = 2$s and the communication delay is 1ms. In addition, the MG PI voltage controllers in both cases have 0.1ms sampling time while the MPC compensator has 2ms sampling time.
- For both systems, the BESS is a Lithium-Ion type. Also, the SC consists of an ideal capacitor with a series internal resistance. It is assumed that the SC has no leakage current. Also, it is assumed that the HESS components (i.e., SC and BESS), and PV are efficiently sized. The parameters of BESS and SC are represented in Table 3. In this experiment, the BESS has 2 hours charge time and SC's charge time is 2 seconds.
- In both test cases, it is assumed that the PV module is in MPPT mode, and it operates as a CPS. Moreover, it is assumed the DC MG supplies a power electronic load (i.e., a load converter) that demands constant power under the varying voltage at MG side, so it operates as a CPL. Thus, the difference between load and PV power (i.e., $P_{CP} = P_L - P_{PV}$) represents the equivalent CPL/CPS (or the net power) that is supplied/absorbed by the HESS. Hence, $P_{CP} > 0$ implies that the HESS is loaded by an equivalent CPL that demands identical power to P_{CP} and tends to destabilize the system [34] (see the dynamics of the MG in (1) and (10)).
- It is assumed that the HESS nominal power and maximum P_{CP} are both 20kW (i.e., $P_{CP}^{\max} = 20$kW). Accordingly, based on the stability analysis provided in section II, in Case 1, the MG voltage controller suffers from low-marginal stability when it operates the "BESS-only" operation. So, the gains of the MG voltage controller are selected as $k_{P3} = 0.75, k_{I3} = 35$ to guarantee the stability of the MG at the nominal CPL (i.e., $P_{CP}^{\max}$). However, based on the stability analysis in section II, the gains of MG voltage controller can be larger in Case 2 (i.e., FB-MPC), so they are defined as $k_{P3} = 1.9, k_{I3} = 72$.

TABLE 2. MPC parameters.

Symbol	Quantity	Value
ψ_e	tracking error's weight	8×10^{-5}
ψ_c	manipulated variable move's weight	0.1
ρ	slack variable's weight	0.002
H_p	prediction horizon	50
H_c	control horizon	10
λ	ECR value	1
T_s	sampling time	2 ms
$SoC_{\min}$	minimum allowable SoC of SC (output constraint)	20%
$SoC_{\max}$	maximum allowable SoC of SC (output constraint)	80%

TABLE 3. HESS parameters.

Symbol	Quantity	Value
Q_n^{SC}	charge capacity of the SC	0.22 A.h
Q_n^b	charge capacity of the BESS	800 A.h
C_{SC}	capacitance of the SC	4.21 F
I_n	nominal current of the SC and BESS	400 A
R_{SC}	internal series resistance of the SC	2 mΩ
R_b	internal series resistance of the BESS	5.3 mΩ
$v_b^{\max}$	nominal terminal voltage of the BESS	55 V
$v_{SC}^{\max}$	nominal terminal voltage of the SC	190 V

As discussed in section I, the sudden load variations or rapid PV power fluctuations (i.e., fast P_{CP} changes), adds a considerable stress on the grid-forming HESSs which may cause over charging/discharging of the SC. So, to evaluate the performance of the FB-MPC method and compare it with conventional FB power allocation strategies, the dynamical behavior of Case 1 (i.e., FB) and Case 2 (i.e., FB-MPC) systems are assessed in three different rapid load (or P_{CP}) variation scenarios. The first scenario contains a sharp shift of P_{CP} from 10kW to 15kW at $t = 10$s and then sharp load reduction from 15kW to 10kW at $t = 25$s. In the second situation, the DC MG experiences a fast and periodic pulsed-shape variation of P_{CP}. In the last condition, P_{CP} sharply increases from 10kW to 19kW at $t = 70$s and then

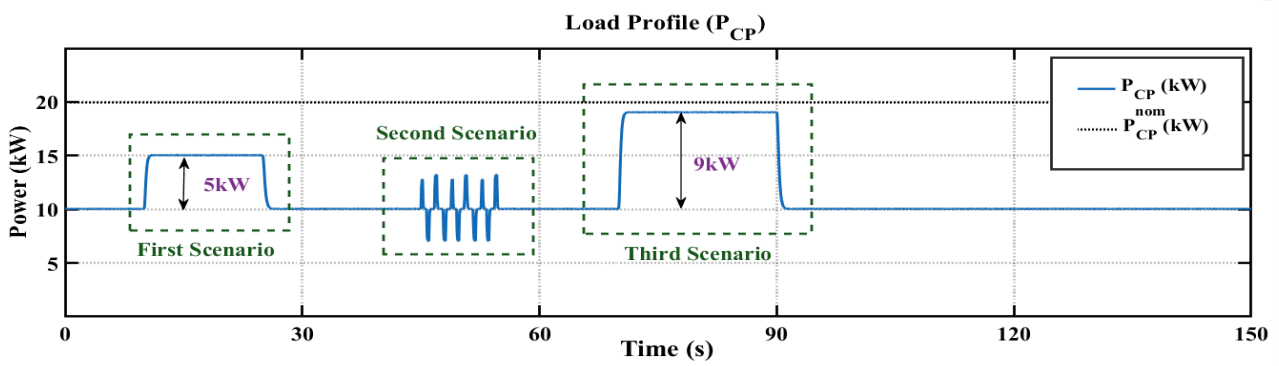

FIGURE 13. The load change scenarios in the test systems.

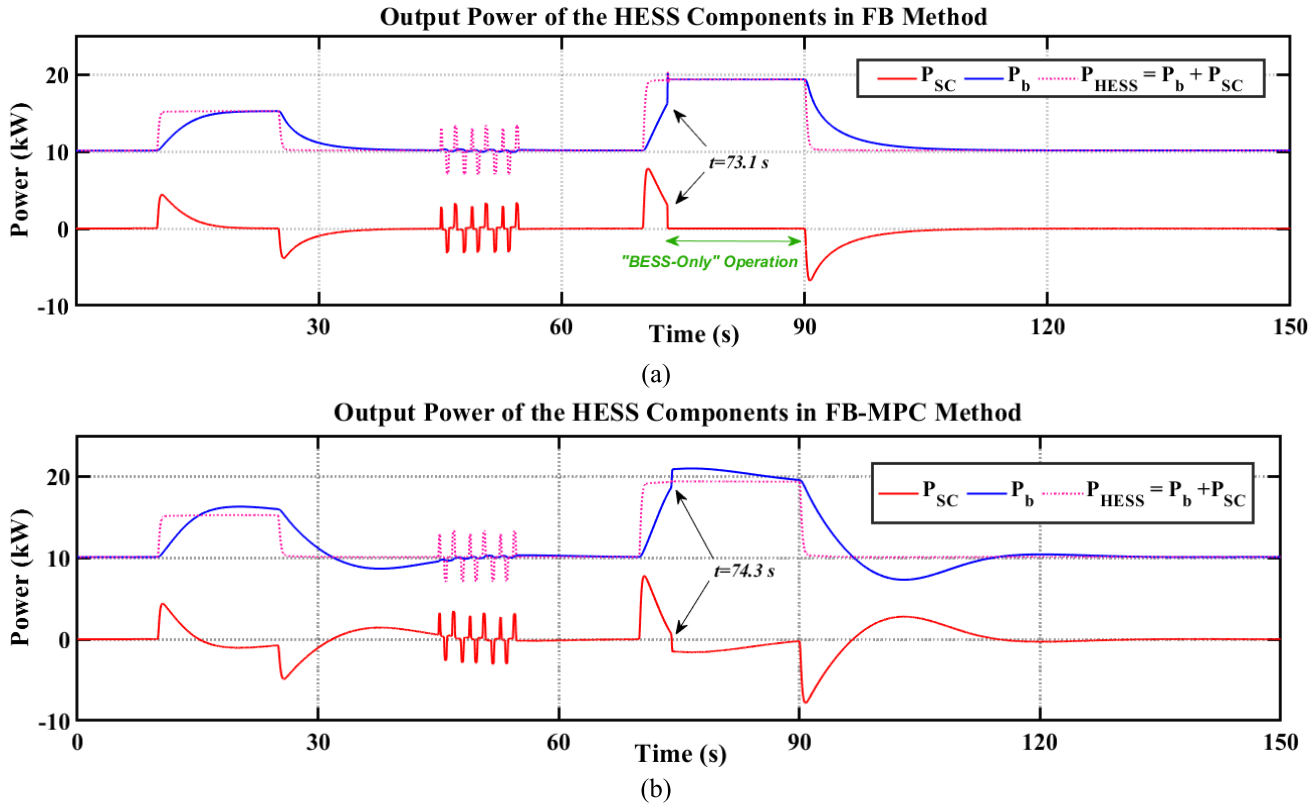

FIGURE 14. The output power of the HESS components in the test cases (a) Case1 (i.e., conventional FB), (b) Case 2 (i.e., the proposed FB-MPC).

decreases from 19kW to 10 kW at $t = 90$s. Fig. 13. illustrates the P_{CP} profile in these three load scenarios. It should be noted that, practically, the first and the third load change scenarios may happen during adding/losing a load/source converter and the second load change scenario is caused by the PPLs (e.g., electric propulsion or laser guns) inside the DC MG.

Fig. 14. shows the output power of the BESS and SC in Case 1 (i.e., FB) and Case 2 (i.e., FB-MPC) systems during the discussed load change scenarios where $P_{SC} > 0$ means that the SC is discharging and $P_{SC} < 0$ shows that the SC is charging. As seen in Fig. 14 (a) and (b), the output power of BESS is smoothed and the high frequency variations of the P_{CP} are allocated to the SC in both FB and FB-MPC methods. Also, the HESS output power (i.e., $P_{HESS} = P_b + P_{SC}$) is equal to the P_{CP} (i.e., $P_{HESS} \simeq P_{CP}$) in both cases that indicates the balance between power generation and load. However, the BESS and SC have slightly different output power profiles in FB-MPC method compared to the FB approach, due to the impact of the MPC compensator.

Fig. 15 represents the transfer power between the BESS and SC in FB-MPC approach due to MPC actions

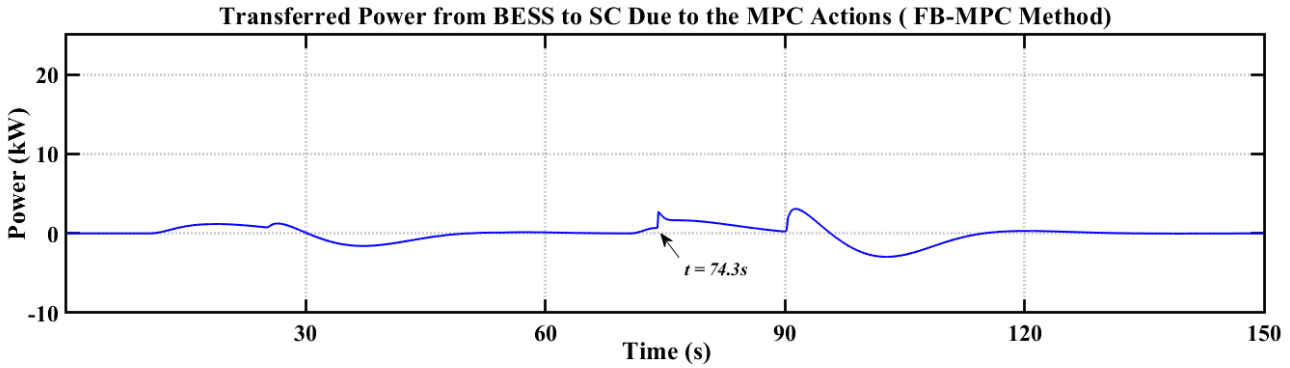

FIGURE 15. Transferred power from BESS to SC because of the MPC actions in the FB-MPC method.

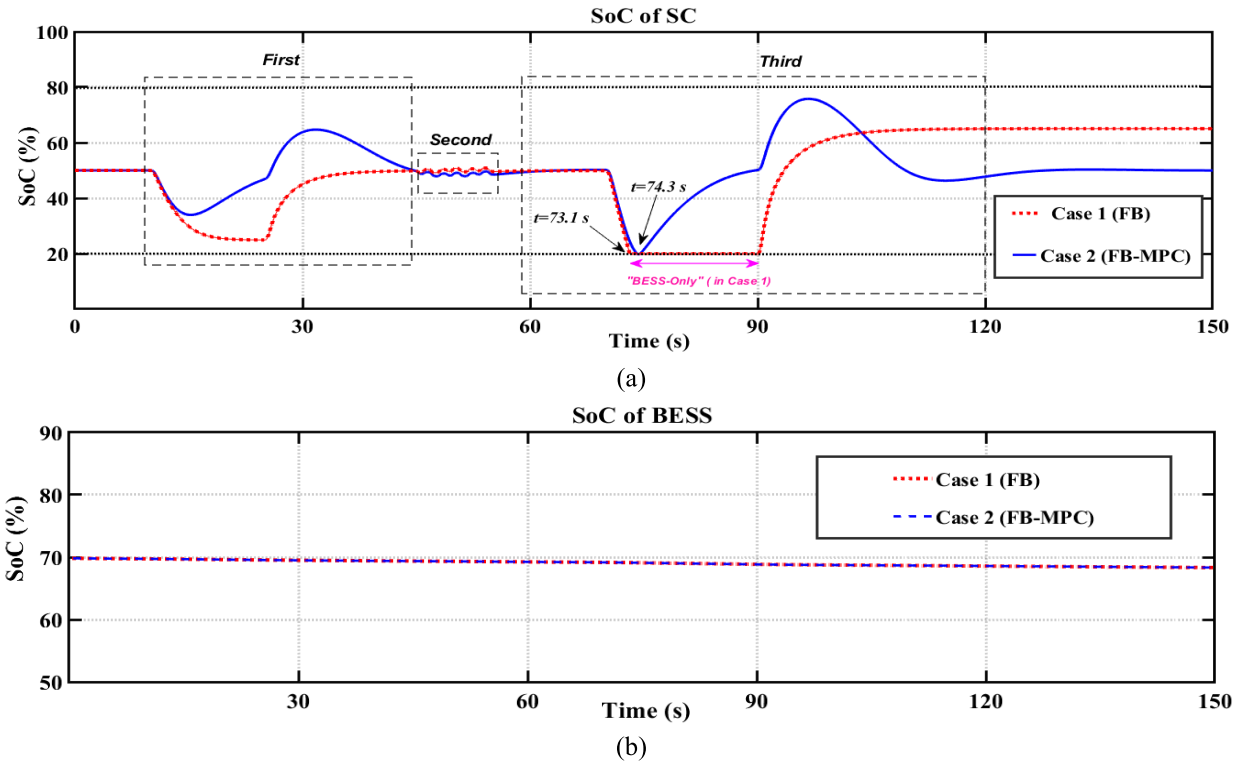

FIGURE 16. The SC and BESS SoC variation (a) SoC of SC, (b) SoC of BESS.

(i.e., compensation power). Fig. 16 also illustrates the SC and BESS SoC variation in Case 1 and Case 2 systems. As seen in Fig. 16(a), in FB-MPC method, MPC compensator provides an additional coordination between BESS and SC in which the BESS gradually charges/discharges the SC and controls its SoC variation in a predefined range. Due to the significant P_{CP} changes in the third load change scenario (see Fig. 13 and Fig. 14), a high amount of power is sent to the SC. So, in FB method, the SoC of SC reaches to its minimum allowable value at $t = 73.1$s (see Fig. 16(a)). Thus, the rule-based supervisory controller deactivates the SC and allocates P_{HESS} power to the BESS (i.e., "BESS-only" operation). Then, at $t = 90$s, the load power suddenly decreases, so the output of the HPF becomes negative (i.e., $i_{HPF} < 0$). Consequently, the rule-based supervisory controller activates the SC and the HESS switches back to "BESS-SC" operating mode (see logic of the rule-based supervisory controller in Fig. 5). In addition, as it can be seen in Fig. 14, deactivating the SC (i.e., switching to "BESS-only" mode) forces the BESS to suddenly change its output power which puts a large stress on the BESS and MG voltage control system. On the other hand, in Case 2 (i.e., FB-MPC), because of the sudden load change at $t = 70$s, the SoC of SC approximately reaches to its minimum value at $t = 74.3$s. At this moment, the MPC

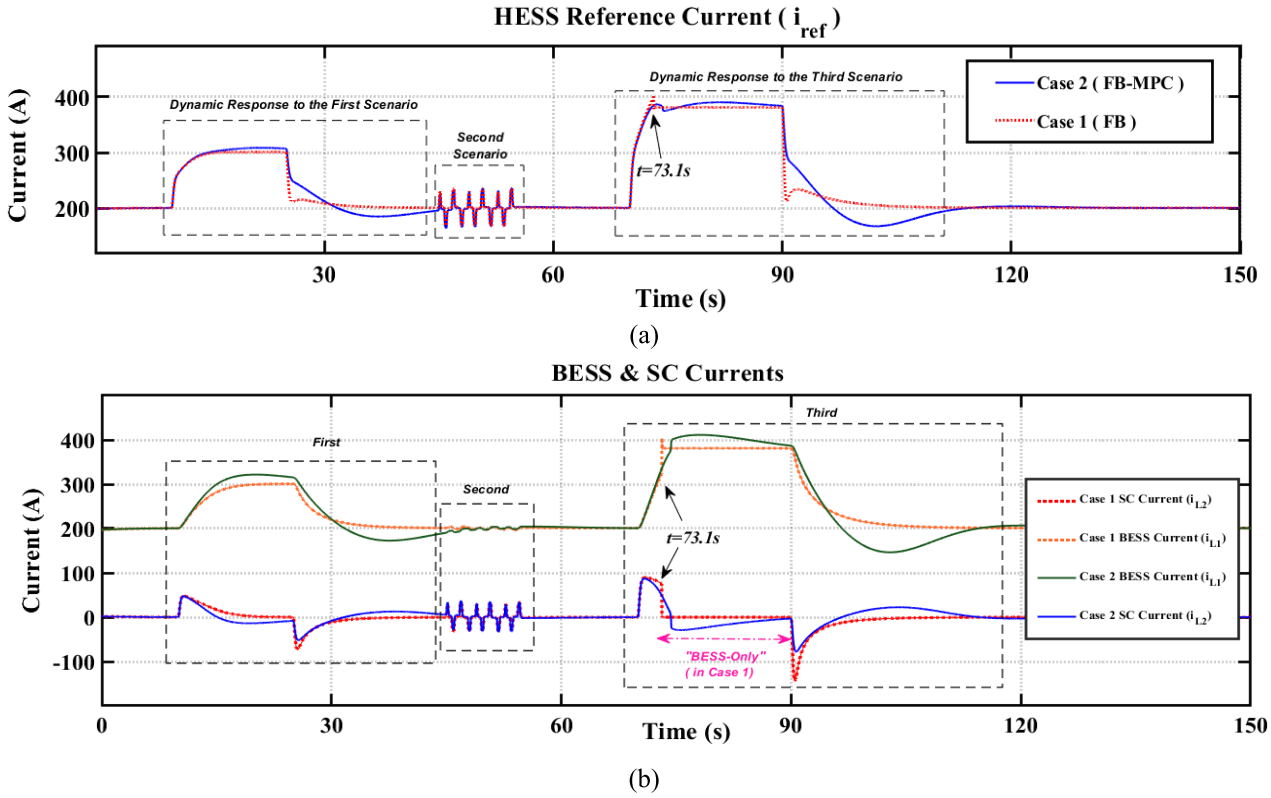

FIGURE 17. The performance of the current allocation systems in the case study MGs (i.e., Case1 and Case 2). (a) HESS reference current (i.e., i_{ref}), (b) The SC and BESS currents (i.e., i_{L1}, i_{L2}).

compensator predicts that there will be a constraint violation in its prediction horizon. So, it shifts the compensator term (i.e., d_{com}), so that force the BESS to react more quickly and charge the SC. This relatively faster movement of the d_{com} (or the BESS output power) at $t = 74.3$s is clearly illustrated in Fig. 14 (b). Consequently, the MPC compensator prevents the SC SoC violation in a switching-less manner. In addition, it can be observed that due to the significantly larger charge time of the BESS (i.e., 2hours), the SoC of BESS remains approximately unchanged during the simulation interval in both cases.

Fig. 17 compares the current allocation performance of the conventional FB (i.e., Case 1) with the proposed FB-MPC technique (i.e., Case 2) in which Fig. 17(a) represents HESS reference currents computed by MG voltage controllers and Fig. 16(b) illustrates the output currents of the HESS components in Case 1 (i.e., FB) and Case 2 (i.e., FB-MPC) systems. As seen, the HPF assigns the high frequency components (i.e., sharp changes) of the reference current to SC, so that smooth out the reference current of BESS. In addition, it can be observed that high frequency pulsed-shape load variations in the second scenario are completely absorbed by the SC in both cases (i.e., Case 1 and Case 2).

In the third load scenario, as discussed before, the SC (or filter) is deactivated at $t = 73.1$s in Case 1 and the HESS switches to the "BESS-only" operation to avoid SC SoC violation. As a result, the SC current is swiftly shifted to zero which can cause a considerable transient voltage sag. However, the proposed FB-MPC method guarantees the continuous operation of SC during the entire system operation by adding a compensation current (i.e., d_{com} defined in equation (31)) to the SC and subtracting that value from the BESS reference current. This value (i.e., d_{com}) is illustrated in Fig. 18. As seen, the d_{com} experiences a relatively fast move when the SoC of SC reaches to its minimum value at $t = 74.3$s. The reason is that, at $t = 73.1$s, the MPC predicts that its output constraint (i.e., the SC SoC allowable range) is going to be violated which results in a small nonzero slack variable (i.e., $\varepsilon \neq 0$) in MPC cost function defined in (28). Considering a large slack variable weight (i.e., ρ), this nonzero slack variable causes a large value in the third term of the MPC cost function. Thus, the MPC compensator quickly reduces the compensation current to minimize the cost function. As a result, the output current of BESS rapidly increases to charge the SC and control its SoC variation.

Fig. 19 depicts the BESS and SC terminal voltages during the simulation interval. As seen, due to the fact that the BESS has significantly larger charge time (i.e., 2hours), the terminal voltage of the BESS (i.e., v_b) remains relatively unchanged during the simulation interval. It is also worth mentioning

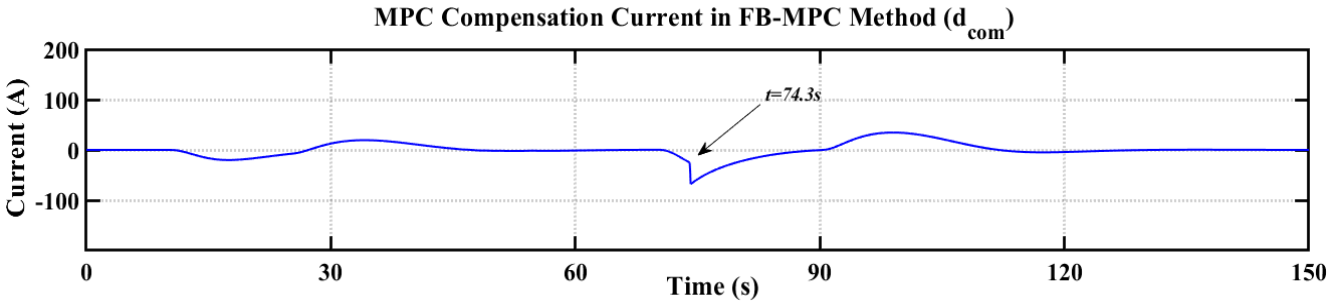

FIGURE 18. The MG DC bus voltage during the load change scenarios.

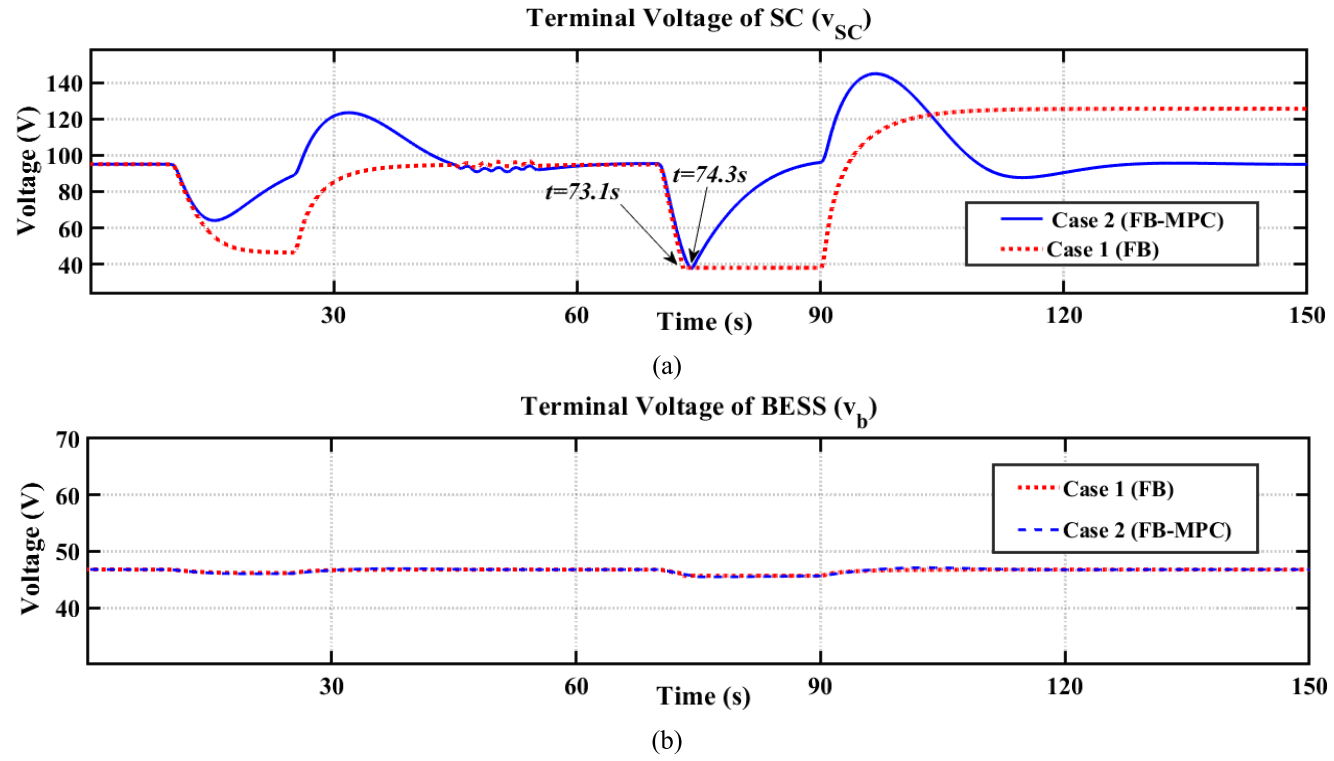

FIGURE 19. The output power of the HESS components in the test cases (a) Case1 (i.e., conventional FB), (b) Case 2 (i.e., the proposed FB-MPC).

that the proposed FB-MPC technique causes different SoC variation in Case 2 compared to the FB method (i.e., Case 1) that results into a different terminal voltage of the SC (i.e., v_{SC}). Thereby, the reference currents of HESSs in Case 1 and Case 2 computed by the MG voltage controller, have relatively different profiles during the system operation (see Fig. 17(a)).

Fig. 20 represents the transient variation of the MG DC bus voltage (i.e., v_{dc}) during the three load change scenarios. As seen, because the MG voltage controller has higher marginal stability and higher gain values in Case 2 (i.e., the FB-MPC method), it can provide faster responses to the load changes which in turn reduces the transient voltage deviations and enhances the MG's voltage quality. In addition, it can be seen that at the switching instance in Case 1 (i.e., $t = 73.1$s), the MG DC bus experiences a significant voltage sag. However, this large transient voltage sag is avoided in the proposed FB-MPC technique, due to its switching/less performance. Instead, under the FB-MPC method, the MG DC bus experiences a very small voltage sage (i.e., 1.7 V) at $t = 74.3$s because of the relatively quick adjustment of d_{com}. This voltage sage is 90% smaller than the voltage sag in FB method and it is fairly negligible. Consequently, the MG DC bus experiences smaller voltage sags (smaller peak and shorter duration) at sudden load changes showing the improvement of the MG voltage quality with the proposed FB-MPC method [37].

Table 4 also compares three voltage quality indexes including the sum of absolute value of voltage changes (SAVC), the integral of the square error (ISE), and the integral

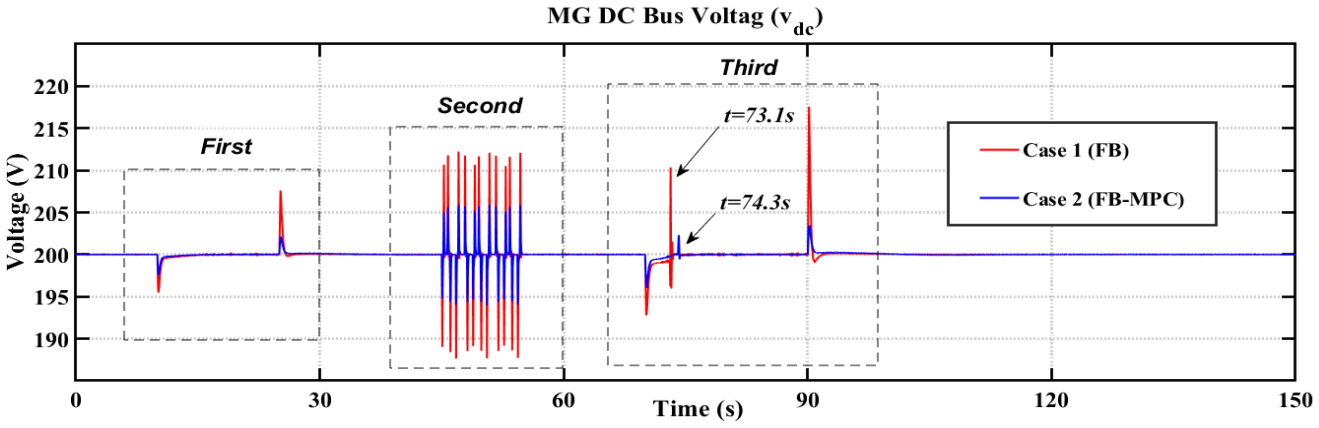

FIGURE 20. The MG DC bus voltage during the load change scenarios.

TABLE 4. Voltage quality indexes.

Index	FB (Case 1)	FB-MPC (Case 2)
ISE	235 (V^2)	55.2 (V^2)
IAE	38.52 (V)	22.46 (V)
SAVC	0.80 (V)	0.38 (V)

of absolute value of error (IAE) which are obtained as

$$\begin{cases} ISE = \int \left(v_{ref} - v_{dc}\right)^2 dt \\ IAE = \int \left|v_{ref} - v_{dc}\right| dt \\ SAVC = \sum_k \left|v_{dc}(kT+T) - v_{dc}(kT)\right|, \ T = 0.1\text{ms} \end{cases} \tag{32}$$

In (32), the lower value of ISE and IAE shows the better voltage regulation performance of the MG voltage control system. In addition, the lower SAVC shows the smaller voltage ripples and flatter voltage profile at MG DC bus. As seen in Table 4, all the indexes (i.e., IAE, ISE, and SAVC) are considerably lower in FB-MPC which indicates the higher voltage quality of MG and better performance of the MG voltage control system under the proposed FB-MPC method.

V. DISCUSSION AND FUTURE RESEARCH

A. THE FB-MPC METHOD IN MULTI-BUS MGS

The simulation results and small-signal stability analysis of this work demonstrates that the proposed FB-MPC approach improves the performance of the primary control layer of a single bus DC MG that contains a grid-forming HESS unit. Consequently, the MG voltage controller can regulate the MG DC bus voltage to its reference (i.e., v_{ref}) value with less transient voltage oscillations at rapid load changes. In this work, the reference voltage for the MG primary controller has a constant value which is exactly equal to the nominal voltage of the single bus DC MG. However, in multi-bus/multi-generation DC MGs, the reference voltages for the primary controllers are typically computed by the secondary control layer of the MG. In such systems, the secondary control layer adjusts the reference voltage of the grid-forming DERs to ensure proportional power sharing between them as well as restoring the steady state voltage of the MG (see the objectives of secondary control layer in Fig. 1). Consequently, reference voltages of the primary controllers may slightly change during the system operation. Nevertheless, the secondary control layer has by far slower dynamics compared to primary control layer (see Fig. 1) which indicates that the secondary control layer does not considerably impact the transient response of the primary controllers or transient voltage stability of the MG. Consequently, the advantages of the proposed FB-MPC method (i.e., improving the transient response of the primary control layer) will be still valid in a DC MG with multiple grid-forming DERs.

Moreover, due to very fast dynamic response of the primary control layer, typically, there is not any communication between primary controllers of grid-forming DERs in a multi-bus/multi-generation MG. In other words, based on the the standard control structure of DC MGs [38], the primary controllers (i.e., convert controllers) just use their local information as well as a reference voltage that is adjusted by the secondary control layer. Consequently, the effective coordination (e.g., power sharing) between the DERs can be provided through the suitable actions of the secondary control layer which may have a centralized or a distributed control architecture [38]. As discussed in section III, the proposed real-time FB-MPC system is located at the primary control layer of MG (i.e., converter controllers) and it does not need the information of other DERs (e.g., PV). Consequently, similar to the conventional control structure of DC MGs, the primary control layer of the HESS unit just requires its local information including the local DC bus voltage, and SC SoC variation. Therefore, the proposed FB-MPC is compatible with the conventional hierarchical control structure of DC

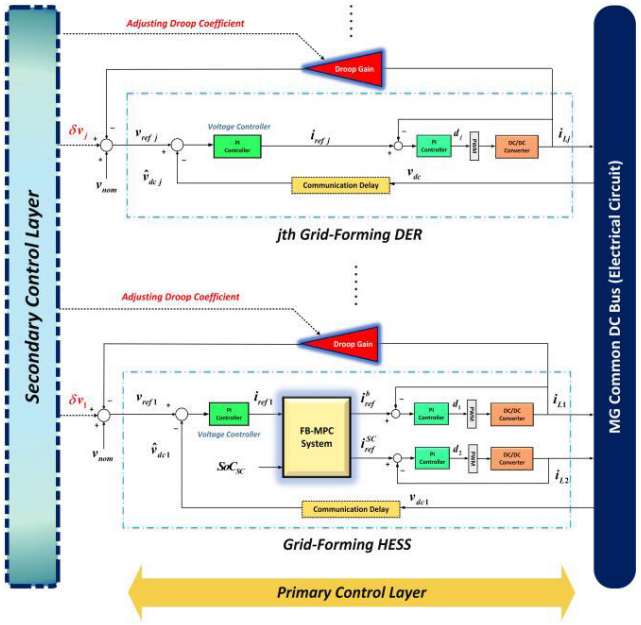

FIGURE 21. The suggested control structure of a DC MG with multiple DERs including a grid-forming HESS with the proposed FB-MPC current allocation system.

MGs, so it can be easily extended into multi-bus/multi-generation systems.

Fig. 21 shows the suggested hierarchical control structure of a DC MG that contains multiple grid-forming DERs including a grid-forming HESS unit. In this structure, the grid-forming HESS utilizes the proposed FB-MPC current allocation system discussed in section III (see Fig. 11). As seen, similar to the conventional hierarchical control structure of MGs [38], the secondary controller selects the reference voltage of the primary controller of DERs including the grid-forming HESS (i.e., v_{refj}) by adjusting the droop gains and adding a voltage restoration term for each DER (i.e., δv_j).

It should be noted that in multiple bus DC MGs, the line impedance (i.e., the impedance of the DC links between DERs) may slightly affect the marginal stability of the system as well as the choice of appropriate gains for PI voltage controllers. In addition, the number of grid-forming HESS units inside the MG, the topology of the DC MG, and types of power electronic converters (e.g., boost, buck, buck-boost) can also alter the dynamic model of the system and slightly impact the marginal stability and transient response of the DC MG.

Consequently, based on the application and the topology of the DC MG, developing a detailed dynamic model of the system and applying further stability analysis can be beneficial. Consequently, a future research direction of this work is to investigate the impact of the discussed parameters (e.g., the line-impedance, MG topology, and the number of grid-forming HESS units with FB-MPC method) on the dynamic stability of a DC MG with multiple DERs.

B. ACTIVE DAMPING OF CPLS WITH FB-MPC METHOD

The stability analysis results of this paper can be discussed from a different perspective. These results show that when the FB current assignment system and SC are activated, the DC MG has higher marginal stability in the presence of CPLs. In addition, increasing the time constant of the filter can improve the transient voltage stability of the DC MG. This means that the instability effect of the CPLs that typically requires active or passive stabilization techniques or more advanced voltage controllers, can be easily addressed by a grid-forming HESS unit in which the size of the filter is appropriately selected, and the continuous operation of SC and filter is guaranteed. Consequently, the other future research direction is to compare the performance of proposed FB-MPC technique with the existing active stabilizers in terms of stability improvement and cost-efficiency for different MG applications.

VI. CONCLUSION

FB strategies are widely used in HESS applications to perform the power/current allocation between the BESS and SC. In these methods, typically, an LTI filter is utilized that splits the HESS reference power/current into high-frequency and low-frequency components and then allocates the high-frequency parts to SC. This paper firstly provides a small-signal stability analysis to investigate the impact of the HESS current assignment filter on the dynamic stability of a single bus DC MG in which a grid-forming HESS supplies a CPL. The stability analysis shows that the current assignment filter improves the marginal stability of the MG. So, the continuous operation of the SC and filter enables the MG PI voltage controller to operate higher gain values as well as tolerating higher communication delays. However, the conventional FB strategies cannot ensure the continuous operation of the SC and filter during the sudden load variations. To address this challenge, this paper proposes an MPC-based SC SoC restoration technique that works in tandem with an LTI filter to perform the current allocation between the BESS and SC. In this method, the MPC controller maintains the SoC of SC in a predefined range, so that ensures the continuous operation of the SC and filter. As a result, the proposed approach indirectly improves the transient response and voltage quality of the system by enabling the MG voltage controller to work with higher gain values. The performance of the proposed FB-MPC method is then validated by simulating a case study DC MG in MATLAB/Simulink.

REFERENCES

[1] M. Fotuhi-Firuzabad, R. Iravani, F. Aminifar, N. Hatziargyriou, and M. Lehtonen, "Guest editorial special section on microgrids," *IEEE Trans. Smart Grid*, vol. 3, no. 4, pp. 1857–1859, Dec. 2012.

[2] M. Ahmed, L. Meegahapola, A. Vahidnia, and M. Datta, "Stability and control aspects of microgrid architectures—A comprehensive review," *IEEE Access*, vol. 8, pp. 144730–144766, 2020.

[3] L. Meng, Q. Shafiee, G. F. Trecate, H. Karimi, D. Fulwani, X. Lu, and J. M. Guerrero, "Review on control of DC microgrids and multiple microgrid clusters," *IEEE J. Emerg. Sel. Topics Power Electron.*, vol. 5, no. 3, pp. 928–948, Sep. 2017.

[4] M. K. Al-Nussairi, R. Bayindir, S. Padmanaban, L. Mihet-Popa, and P. Siano, "Constant power loads (CPL) with microgrids: Problem definition, stability analysis and compensation techniques," *Energies*, vol. 10, no. 10, p. 1656, Oct. 2017.
[5] O. Lorzadeh, I. Lorzadeh, M. N. Soltani, and A. Hajizadeh, "Source-side virtual RC damper-based stabilization technique for cascaded systems in DC microgrids," *IEEE Trans. Energy Convers.*, vol. 36, no. 3, pp. 1883–1895, Sep. 2021.
[6] M. Hassan, M. Worku, A. Eladl, and M. Abido, "Dynamic stability performance of autonomous microgrid involving high penetration level of constant power loads," *Mathematics*, vol. 9, no. 9, p. 922, Apr. 2021.
[7] Q. Xu, N. Vafamand, L. Chen, T. Dragicevic, L. Xie, and F. Blaabjerg, "Review on advanced control technologies for bidirectional DC/DC converters in DC microgrids," *IEEE J. Emerg. Sel. Topics Power Electron.*, vol. 9, no. 2, pp. 1205–1221, Apr. 2021.
[8] Y. Wang, L. Wang, M. Li, and Z. Chen, "A review of key issues for control and management in battery and ultra-capacitor hybrid energy storage systems," *eTransportation*, vol. 4, May 2020, Art. no. 100064.
[9] A. A. K. Arani, G. B. Gharehpetian, and M. Abedi, "Review on energy storage systems control methods in microgrids," *Int. J. Electr. Power Energy Syst.*, vol. 107, pp. 745–757, May 2019.
[10] M. E. Şahin and F. Blaabjerg, "A hybrid PV-battery/supercapacitor system and a basic active power control proposal in MATLAB/simulink," *Electronics*, vol. 9, no. 1, p. 129, Jan. 2020.
[11] S. Hajiaghasi, A. Salemnia, and M. Hamzeh, "Hybrid energy storage system for microgrids applications: A review," *J. Energy Storage*, vol. 21, pp. 543–570, Feb. 2019.
[12] N. R. Tummuru, U. Manandhar, A. Ukil, H. B. Gooi, S. K. Kollimalla, and S. Naidu, "Control strategy for AC-DC microgrid with hybrid energy storage under different operating modes," *Int. J. Electr. Power Energy Syst.*, vol. 104, pp. 807–816, Jan. 2019.
[13] V. T. Nguyen and J. W. Shim, "Virtual capacity of hybrid energy storage systems using adaptive state of charge range control for smoothing renewable intermittency," *IEEE Access*, vol. 8, pp. 126951–126964, 2020.
[14] W. Jing, C. H. Lai, W. S. H. Wong, and M. L. D. Wong, "Dynamic power allocation of battery-supercapacitor hybrid energy storage for standalone PV microgrid applications," *Sustain. Energy Technol. Assessments*, vol. 22, pp. 55–64, Aug. 2017.
[15] X. Lu, Y. Chen, M. Fu, and H. Wang, "Multi-objective optimization-based real-time control strategy for battery/ultracapacitor hybrid energy management systems," *IEEE Access*, vol. 7, pp. 11640–11650, 2019.
[16] X. Chang, Y. Li, X. Li, and X. Chen, "An active damping method based on a supercapacitor energy storage system to overcome the destabilizing effect of instantaneous constant power loads in DC microgrids," *IEEE Trans. Energy Convers.*, vol. 32, no. 1, pp. 36–47, Mar. 2017.
[17] S. Kotra and M. K. Mishra, "Design and stability analysis of DC microgrid with hybrid energy storage system," *IEEE Trans. Sustain. Energy*, vol. 10, no. 3, pp. 1603–1612, Jul. 2019.
[18] P. Singh and J. S. Lather, "Power management and control of a grid-independent DC microgrid with hybrid energy storage system," *Sustain. Energy Technol. Assessments*, vol. 43, Feb. 2021, Art. no. 100924.
[19] S. A. G. K. Abadi and A. Bidram, "A distributed rule-based power management strategy in a photovoltaic/hybrid energy storage based on an active compensation filtering technique," *IET Renew. Power Gener.*, vol. 15, no. 15, pp. 3688–3703, Nov. 2021.
[20] Q. Xu, X. Hu, P. Wang, J. Xiao, P. Tu, C. Wen, and M. Y. Lee, "A decentralized dynamic power sharing strategy for hybrid energy storage system in autonomous DC microgrid," *IEEE Trans. Ind. Electron.*, vol. 64, no. 7, pp. 5930–5941, Jul. 2017.
[21] U. B. Tayab, M. A. Roslan, L. J. Hwai, and M. Kashif, "A review of droop control techniques for microgrid," *Renew. Sustain. Energy Rev.*, vol. 76, pp. 717–727, Sep. 2017.
[22] J. Hu, Y. Shan, J. M. Guerrero, A. Ioinovici, K. W. Chan, and J. Rodriguez "Model predictive control of microgrids—An overview," *Renew. Sust. Energ. Rev.*, vol. 136, Feb. 2021, Art. no. 110422.
[23] P. Karamanakos, E. Liegmann, T. Geyer, and R. Kennel, "Model predictive control of power electronic systems: Methods, results, and challenges," *IEEE Open J. Ind. Appl.*, vol. 1, pp. 95–114, 2020.
[24] U. R. Nair and R. Costa-Castello, "A model predictive control-based energy management scheme for hybrid storage system in islanded microgrids," *IEEE Access*, vol. 8, pp. 97809–97822, 2020.
[25] X. Zhang, B. Wang, D. Gamage, and A. Ukil, "Model predictive and iterative learning control based hybrid control method for hybrid energy storage system," *IEEE Trans. Sustain. Energy*, vol. 12, no. 4, pp. 2146–2158, Oct. 2021.
[26] H. Chen, R. Xiong, C. Lin, and W. Shen, "Model predictive control based real-time energy management for hybrid energy storage system," *CSEE J. Power Energy Syst.*, vol. 7, no. 4, pp. 862–874, Jul. 2021.
[27] Z. Jia, J. Jiang, H. Lin, and L. Cheng, "A real-time MPC-based energy management of hybrid energy storage system in urban rail vehicles," *Energy Proc.*, vol. 152, pp. 526–531, Oct. 2018.
[28] F. Garcia-Torres, L. Valverde, and C. Bordons, "Optimal load sharing of hydrogen-based microgrids with hybrid storage using model-predictive control," *IEEE Trans. Ind. Electron.*, vol. 63, no. 8, pp. 4919–4928, Aug. 2016.
[29] F. Ni, Z. Zheng, Q. Xie, X. Xiao, Y. Zong, and C. Huang, "Enhancing resilience of DC microgrids with model predictive control based hybrid energy storage system," *Int. J. Electr. Power Energy Syst.*, vol. 128, Jun. 2021, Art. no. 106738.
[30] A. Ebrahimian, S. Vahid, N. Weise, and A. El-Refaie, "Two level AC-DC-AC converter design with a new approach to implement finite control set model predictive control," in *Proc. 22nd IEEE Int. Conf. Ind. Technol. (ICIT)*, Mar. 2021, pp. 514–520.
[31] M. Aguirre, S. Kouro, C. A. Rojas, J. Rodriguez, and J. I. Leon, "Switching frequency regulation for FCS-MPC based on a period control approach," *IEEE Trans. Ind. Electron.*, vol. 65, no. 7, pp. 5764–5773, Jul. 2018.
[32] Z. Karami, Q. Shafiee, S. Sahoo, M. Yaribeygi, H. Bevrani, and T. Dragicevic, "Hybrid model predictive control of DC–DC boost converters with constant power load," *IEEE Trans. Energy Convers.*, vol. 36, no. 2, pp. 1347–1356, Jun. 2021.
[33] S. Singh, A. R. Gautam, and D. Fulwani, "Constant power loads and their effects in DC distributed power systems: A review," *Renew. Sustain. Energy Rev.*, vol. 72, pp. 407–421, May 2017.
[34] X. Lu, K. Sun, J. M. Guerrero, J. C. Vasquez, L. Huang, and J. Wang, "Stability enhancement based on virtual impedance for DC microgrids with constant power loads," *IEEE Trans. Smart Grid*, vol. 6, no. 6, pp. 2770–2783, Nov. 2015.
[35] H. R. Baghaee, M. Mirsalim, G. B. Gharehpetian, and H. A. Talebi, "A generalized descriptor-system robust H_∞ control of autonomous microgrids to improve small and large signal stability considering communication delays and load nonlinearities," *Int. J. Electr. Power Energy Syst.*, vol. 92, pp. 63–82, Nov. 2017.
[36] K. Gu, J. Chen, and V. Kharitonov, *Stability of Time-Delay Systems*. Boston, MA, USA: Springer, 2003.
[37] G. Van den Broeck, J. Stuyts, and J. Driesen, "A critical review of power quality standards and definitions applied to DC microgrids," *Appl. Energy*, vol. 229, pp. 281–288, Nov. 2018.
[38] Y. Han, X. Ning, P. Yang, and L. Xu, "Review of power sharing, voltage restoration and stabilization techniques in hierarchical controlled DC microgrids," *IEEE Access*, vol. 7, pp. 149202–149223, 2019.

SEYYED ALI GHORASHI KHALIL ABADI (Graduate Student Member, IEEE) was born in Mashhad, Iran, in 1990. He received the B.S. degree from the Ferdowsi University of Mashhad, Mashhad, in 2014, and the M.S. degree from the Amirkabir University of Technology, Tehran, Iran, in 2017, both in electrical engineering-control. He is currently pursuing the Ph.D. degree with The University of New Mexico, Albuquerque, USA. His main research interests include control and management of DC microgrids, model predictive control, supervisory control, hybrid energy storage systems, and modeling, simulation, and control of complex dynamical systems. He was awarded the Outstanding Student Certificate by the Amirkabir University of Technology, in 2017.

SEYED IMAN HABIBI (Graduate Student Member, IEEE) received the B.Sc. and M.Sc. degrees in electrical engineering from the K. N. Toosi University of Technology, Tehran, Iran, in 2015 and 2018, respectively. He is currently pursuing the Ph.D. degree with The University of New Mexico. His main research interests include secondary control of microgrids, supervisory control, switching control, and adaptive systems.

TOHID KHALILI (Graduate Student Member, IEEE) received the B.Sc. degree from Urmia University, Urmia, Iran, in 2016, and the M.Sc. degree from the University of Tabriz, Tabriz, Iran, in 2018, both in electrical engineering (power systems). He is currently pursuing the Ph.D. degree (Research Assistant) with the Electrical and Computer Engineering Department, The University of New Mexico, Albuquerque, NM, USA. He is the author or coauthor of several journals and conference papers. His main research interests include optimization, reliability, robustness, resiliency, and protection of power systems, power systems operation, demand response programs, renewable energy, energy storage systems, smart grid, evolutionary algorithms, and power systems economic. He serves as a reviewer for several journals.

ALI BIDRAM (Senior Member, IEEE) received the B.Sc. and M.Sc. degrees from the Isfahan University of Technology, Iran, in 2008 and 2010, respectively, and the Ph.D. degree from the University of Texas at Arlington, USA, in 2014.

He is currently an Assistant Professor with the Electrical and Computer Engineering Department, The University of New Mexico, Albuquerque, NM, USA. Before joining The University of New Mexico, he worked with Quanta Technology, LLC, and was involved in a wide range of projects in electric power industry. Such research efforts are culminated in a book, several journal articles in top publication venues and papers in peer-reviewed conference proceedings, and technical reports. His research interest includes control and coordination of energy assets in power electronics-intensive energy distribution grids. His area of expertise lies within control and coordination of energy assets in power electronics-intensive energy distribution grids. Such research efforts are culminated in a book, several journal papers in top publication venues and articles in peer-reviewed conference proceedings, and technical reports. He has received the IEEE Albuquerque Section Outstanding Engineering Educator Award, the New Mexico EPSCoR Mentorship Award, the University of Texas at Arlington N. M. Stelmakh Outstanding Student Research Award, the Quanta Technology Shooting Star Award, the IEEE Kansas Power and Energy Conference Best Paper Award, and the cover article of December 2014 in IEEE Control Systems. He is an Associate Editor of the IEEE TRANSACTIONS ON INDUSTRY APPLICATIONS.